Sensors & Diagnostics

ROYAL SOCIETY OF CHEMISTRY

CRITICAL REVIEW

View Article Online
View Journal | View Issue

Cite this: *Sens. Diagn.*, 2022, **1**, 902

Recent development in carbon dot-based gas sensors

Swathilakshmi and S. Anandhan *

Carbon dots (CDs) are novel 0D nanomaterials discovered in the beginning of the 21st century. They have versatile properties due to which they have gained attention from researchers to successfully develop a wide variety of devices. Among them, one of the foremost is developing sensors capable of real-time detection of ultra-low concentration of gas molecules using CDs as an active sensor material. Gas sensors have both industrial and medical significance. Hence, in recent years more and more work has been carried out for developing gas sensors with good reproducibility and stability and high selectivity, sensitivity, response rate and recovery rate. Although several metal oxides and mesoporous materials have been developed to play the role of sensitive film, these materials have been found to be lacking in certain aspects. Addition of a uniformly dispersed CD film over metal oxide nanostructures, conducting polymers or mesoporous materials has enabled us to overcome their limitations. Here, we attempt to summarize the imperative role of CDs as an active material in gas sensors as we briefly discuss some of the synthesis routes. A detailed account on the optical and electrical properties of CDs and the recent developments in CD-based gas sensors is provided here.

Received 26th April 2022,
Accepted 10th July 2022

DOI: 10.1039/d2sd00074a

rsc.li/sensors

1. Introduction

Carbon dots (CDs) are generally quasi-spherical nanoparticles that consist of sp^2 or sp^3 carbon, oxygen or/and nitrogen-based groups and post-modified chemical groups forming an amorphous to crystalline structure.[1,2] CDs were first discovered by Xu *et al.* during the purification of single walled carbon nanotubes by agarose gel and glass bead electrophoresis in 2004.[3] Recently, CDs have been gaining a great deal of attention as they possess several advantages over quantum dots such as low cost, simple synthesis routes using renewable precursors, easy modifiability, low cytotoxicity, benign biocompatibility, high photostability and hydrophilicity.[2,4–8] Most of these properties are associated with the surface state while some are associated with the core of CDs.[9] CDs can be prepared by several methods, including arc discharge, electrochemical oxidation, laser ablation and various thermal-based methods, such as pyrolysis, hydrothermal and microwave assisted techniques.[6] CDs may contain either a completely amorphous structure[10] or a crystalline core with an amorphous shell, depending on the synthesis route adopted.[11] CDs are further classified based on their carbon core structure into (Fig. 1): carbon nanodots (CNDs), consisting of amorphous quasi-spherical nanodots without proper quantum confinement but that entails a high degree of carbonization; carbon quantum dots (CQDs), consisting of crystalline spherical quantum dots with quantum confinement; and graphene quantum dots (GQDs) consisting of π-conjugated 0D structure made up of single or few layer graphene with a lateral size restricted to less than 20 nm.[6,12–14] Recently, another group of CDs namely carbonized polymer dots (CPDs) was introduced. CPDs are a carbon/polymer hybrid 0D nanomaterial that consists of a carbon core surrounded by a framework of crosslinked polymer chains on its surface.[12,13,15,16] Also, CDs with different morphologies such as triangularly shaped CDs with narrow size distributions have been produced.[9,17]

The major difference between GQDs and graphene is that graphene as a 2D structure has zero bandgap while by minimizing the lateral size of graphene to nm in 0D GQDs, the edge effect and quantum confinement can increase their band gap at the UV regime.[2,13] GQDs have a larger surface to volume ratio, more functional groups on their surface, and interlayer defects and edges, thus more active sites for adsorption of chemicals than graphene.[13,18–20] As a result, GQDs exhibit the advantageous properties of both graphene and quantum dots.[6,21,22] CDs have been used as innocuous optical imaging probes and for sensing in solution or solid phase, as they exhibit excellent luminescence properties.[6,23] They are extensively used for bioimaging, theranostics, target drug

Department of Metallurgical and Materials Engineering, National Institute of Technology-Karnataka, Surathkal, Srinivasnagar (P.O.), Mangaluru, 575025, India. E-mail: anandhan@nitk.edu.in, anandtmg@gmail.com

delivery, biosensing[2,9,24–26] and tissue engineering,[1] photovoltaics, supercapacitors, lithium ion batteries,[13,19,21,27–29] LEDs,[30,31] photocatalysts,[9,14] electrocatalysts[13,15,32] and catalysts for polymerization.[7] Moreover, addition of CQDs as nanofillers was found to improve the piezoelectric response of PVDF by increasing the β-phase content and crystallinity. This further

Swathilakshmi

Swathilakshmi received her BTech in Metallurgical and Materials Engineering from the National Institute of Technology Karnataka, Surathkal, India in 2021. She received the acclaimed Institute Medal, Karthik Alloys Gold Medal, Prof. H. V. Sudhaker Nayak Gold Medal, SMIORE Gold Medal and 1986 Batch Gold Medal in the 19th Annual Convocation of the 2020–2021 graduating batch. She also received the 2021 Indian Institute of Metals-Students' Prize for securing the highest marks in order of merit in the final BTech examination during 2020–2021 academic session among all NITs/Indian Universities/Engineering Colleges. Her research interest includes application of carbon nanomaterials for sensors and optoelectronic devices and understanding the underlying physical phenomena in energy harvesting and energy storage devices by performing first principles calculations.

S. Anandhan

Prof. Anandhan holds a BSc in Chemistry (Madurai Kamaraj University, India, 1995), MSc in Applied Chemistry (Madurai Kamaraj University, India, 1997), MTech in Polymer Technology (Cochin University of Science and Technology, India, 1999) and PhD in Polymer Science and Technology (Indian Institute of Technology Kharagpur, 2004). He was a gold medalist in both BSc and MSc. He was invited as a Visiting Research Associate by the School of Materials Science and Engineering, the University of New South Wales, Australia in 2002. He was a Postdoctoral Fellow and Lecturer in Inha University, Korea (2004–2005) in the erstwhile Textile Engineering Department (currently Chemical Engineering). Subsequently, he served as an Assistant Professor in the Department of Materials Science at AIMST University, Malaysia during 2005–2008. He joined his present organization (National Institute of Technology Karnataka) in 2009 as an Assistant Professor and rose in ranks as Associate Professor and Professor in 2012 and 2018, respectively. He has been teaching courses in the areas of polymers, nanomaterials, materials characterization, and nanocomposites. Under his mentorship, 8 students have earned their doctoral degrees so far and a few more have been working towards their PhD. He has also guided 41 master's research projects in various areas related to polymers and nanotechnology. He has published 85 articles in peer reviewed international journals and his publications have so far received about 1600 citations. He has also published a patent, 3 books and 14 book chapters. He was the principal investigator of 2 sponsored research projects. He is currently a member of the teams that have secured highly competitive research grants from the Department of Science & Technology (DST), India and National Science Foundation, USA. He has been a referee for more than 50 international journals of repute. He has refereed a number of doctoral dissertations from India and abroad. Anandhan has been admitted as a Fellow of the Royal Society of Chemistry (FRSC), UK in September 2021 for his outstanding contribution to the advancement of the chemical sciences through his research on Advanced Functional Nanofibers, Energy Materials, Polymer Blends and Nanocomposites. He has won a number of awards and honours such as Doctoral Research Fellowship from DST-India, Australia-India Council Fellowship, Postdoctoral Fellowship from Inha University-Korea, ARCNN-ARNAM Fellowship from UNSW-Australia, and Fast Track Award for Young Scientists from DST-India. Earlier, he was Elected Fellow of the Institution of Engineers (India) and Indian Chemical Society in 2017 and 2019, respectively.

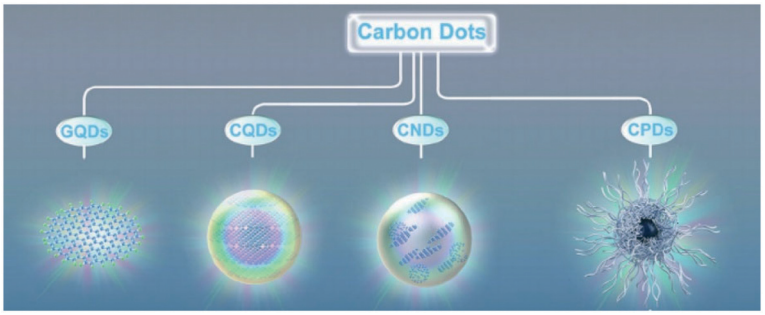

Fig. 1 Classification of CDs.[12] Reproduced with permission from ref. 12, copyright, 2019, Wiley-VCH.

broadens the application field of CDs to low frequency small acceleration detectors for seismic prediction, as well as self-powered and wearable electronics.[33] CD-based polymer coating has been developed to serve as self-healing anti-corrosion coating.[34,35]

As CDs have improved stability, their sensitivity and selectivity can be controlled *via* surface passivation and they can be produced by green synthesis routes, they are extensively studied as active materials for sensors as seen by the rise in the amount of paper published on carbon dot-based sensors in Fig. 2a. A sensor is a kind of transducer which converts chemical information on concentration of a particular molecule into electrical or optical signals. Carbon dots have been used to detect several metal ions such as

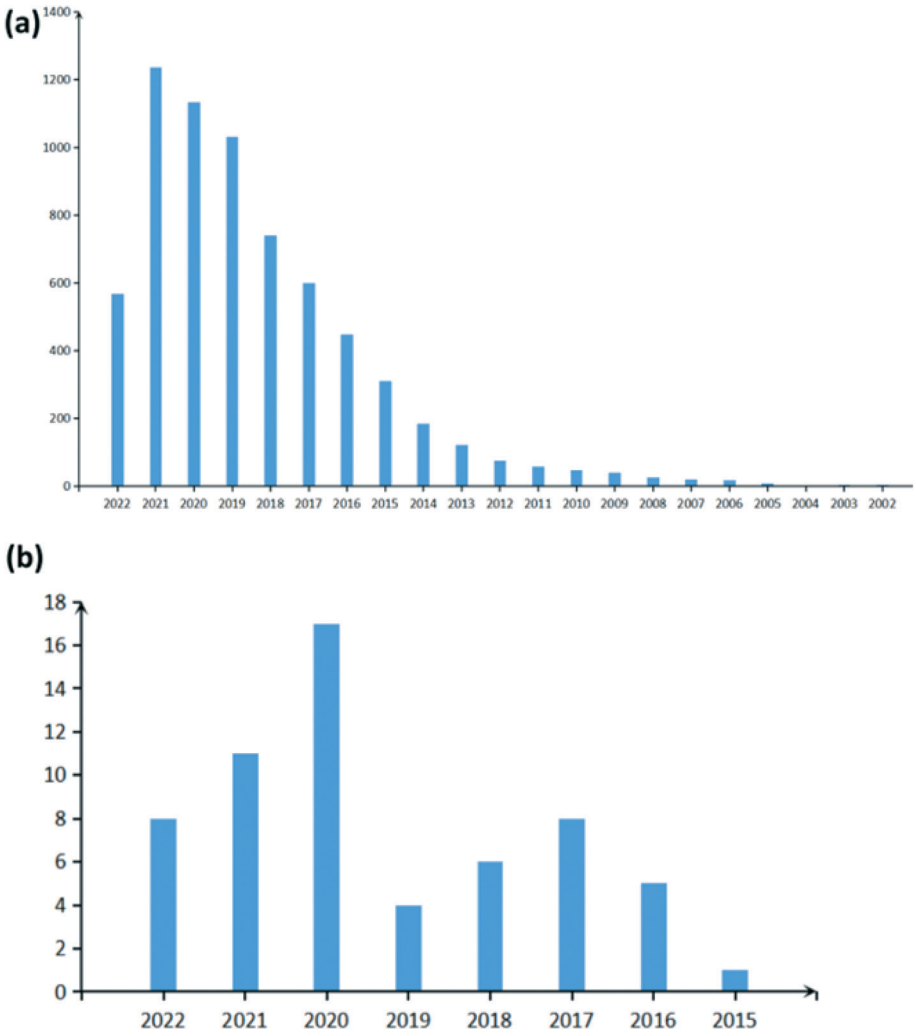

Fig. 2 Statistics of the number of papers published on (a) carbon dot-based sensors (raw data) and (b) carbon dot-based gas sensors (filtered data) as obtained from Web of Science.

Fe^{3+},[13,14,24,36–43] Hg^{2+},[13,16,24,38,40,41,44] Cu^{2+},[13,16,24,38–41,43,45,46] Ag^{+},[13,39,40,43] Pb^{2+},[14,38–40,43] Cr^{6+} (ref. 13, 16, 24, 41 and 47) and so on, relative humidity,[13,48–50] temperature,[37] molecules in the liquid phase,[13,23,51,52] gas molecules, *etc.* Fluorescence sensors,[42,47,53,54] electrochemical sensors[54–58] and colorimetric sensors[43,46,54,59] are some of the widely explored CD-based sensor types. A fluorescence sensor uses variation in the fluorescence intensity/quenching of CDs on absorption and desorption of analytes, while colorimetric sensors use the shift in fluorescence peak of CDs as a sensing signal. Optical sensors are attractive as they are simple, cost effective and provide rapid qualitative information as their results for various chemical species can be observed on-site with the naked eye.[43,46] Unlike fluorescence and colorimetric sensors, which depend on the visual signals, the variation in the resistance or impedance of CDs deposited on glass carbon electrodes is used to detect analytes in electrochemical sensors. These classes of sensors have also been adopted for sensing gas molecules. However, recently the conductometric type of CD-based gas sensor has been gaining attention.

Several industrial effluents and volatile organic compounds in air are toxic to humans and may pose serious health risk to humans and animals. Thus, gas sensors developed must have high selectivity, stability, and reproducibility and must provide warnings at concentrations well below the toxicity level.[60,61] Although other carbon nanomaterials such as carbon nanotubes,[62] graphitic carbon nitride[63] and graphene[64] have been studied as novel sensor materials, they have either poor selectivity, slow response or a small bandgap (low on–off current ratios) and are hence not suitable for detecting trace amounts of gas.[62,64–66] CD-based gas sensors have been shown to meet all the requirements to detect ultra-low concentration of gas molecules with the added advantage of ease of synthesis. Generally, CDs have been used in conjunction with metal oxides, conducting polymers and mesoporous metal organic frameworks to further increase their sensitivity to target gas molecules. Research on CD-based gas sensors is still in its infancy as seen by the very recent rise in the number of papers published in this field (Fig. 2b). In this review, we aim to provide a thorough account of the research carried out till date in CD-based gas sensors and hope to encourage further research. Here, we briefly introduce some of the popular synthesis techniques for CDs followed by a detailed discussion on their optical and electrical properties adopted as signals for detecting gas molecules in sensors. Subsequently, a crude classification of CD-based gas sensors into different classes on the basis of the detection signal is provided. Finally, we provide a brief overview of the importance and application of CD-based gas sensors in the society.

2. Synthesis of carbon dots

Almost any carbon containing material can be used to synthesize CDs. –OH, –COOH and $–NH_2$ groups are important for effective synthesis of CDs. Synthesis of CDs is crudely categorized into top-down and bottom-up approaches.

2.1 Top-down approach

In the top-down approach, CDs are obtained by breaking down or fragmenting carbonaceous materials (Fig. 3a) by acid treatment, ultrasonic method, hydrothermal or solvothermal exfoliation, arc discharge, laser ablation, electrochemical method, *etc.* In the arc discharge process, on generation of

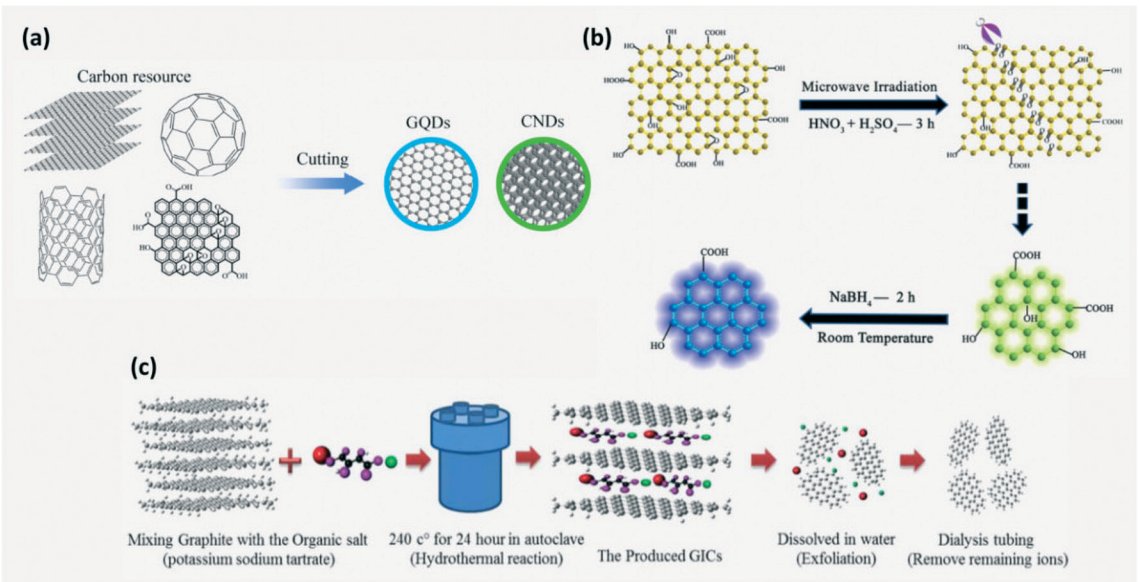

Fig. 3 (a) Schematic of the top-down approach. Reproduced with permission from ref. 13, copyright, 2020, Royal Society of Chemistry. (b) Synthesis of GQDs by a microwave assisted modified Hummer's method. Reproduced with permission from ref. 8, copyright, 2012, Wiley-VCH. (c) Synthesis of GQDs by a hydrothermal exfoliation method.[30] Reproduced with permission from ref. 12, copyright, 2020, Institute of Physics.

plasma, an arc is struck between the anode made up of carbon precursors and the cathode where the carbon vapors aggregate and cool down. But this technique has poor yield.[4,15] Heteroatom doped CDs can be prepared by this method. For example, B,N-co-doped CQDs were synthesized by arc discharge between graphite electrodes and chemical shearing in a controlled atmosphere of H_2 + He + B_2H_6 or H_2 + He + NH_3.[16] In laser ablation, a high pulse laser is irradiated on the target surface to vaporize the precursor to the plasma state which then crystallizes into CQDs and is dispersed in appropriate organic solvents to functionalize its surface. Either a single pulsed or double pulsed laser may be used to ablate, although a second pulse in double pulsed lasers helps in higher ablation of CQDs to smaller size. The downside is that they require complicated equipment, post processing steps and stringent experimental conditions.[15,16] In the case of acid exfoliation, strong acids such as HNO_3 or H_2SO_4 are used to oxidize and cleave graphite, graphene oxides, coal and other carbon materials and simultaneously introduce functional groups.[2,4,15] Chen *et al.* produced GQDs by ball milling MWNTs initially and then subjecting them to acidic oxidation in sonicated H_2SO_4 + HNO_3 solution. The as obtained oxidized GQDs may be further reduced.[2,19] The ultrasonic assisted liquid phase exfoliation technique was developed recently to improve the efficiency of CD production where ultrasonic waves help break carbon materials into nanoparticles in acid, alkali solutions or oxidants.[4,13,16] Although ultrasound assisted methods have the lucrative characteristics of being a simple and time saving process without a need for post-treatment, CDs produced have low quantum yield (QY).[16] Hydrothermal exfoliation involves a reaction between carbonaceous precursors and organic salts dissolved in water in a vacuum autoclave at high temperature for several hours to produce intermediate compounds such as graphite intercalated compounds (GICs). GICs are further broken down to GQDs and purified by filtration followed by dialysis as shown in Fig. 3c.[18,30]

GQDs can be prepared by an electrochemical method where graphite rods or carbon nanotubes (CNTs) are electrolyzed in an appropriate electrolyte with an appropriate counter and reference electrode which controls the type and extent of surface functionalization.[2,9,16,67] Shen *et al.* synthesized GQDs and other carbon nanomaterials by using a diluted ionic liquid (IL) as electrolyte which helps in improving the yield through IL intercalation and oxidative cleavage.[2] But it requires high potential electrolytes and complicated purification steps.[16] A modified Hummer's method along with microwave assistance was developed to produce GQDs where cleaving and reduction of carbon precursors dissolved in strong acids occurs under microwave irradiation resulting in rapid and uniform heating of the reaction medium (Fig. 3b).[8] Although the top down approach is simple and less expensive, it provides poor control of the size and chemical homogeneity of synthesized CDs.[2,15,16,21,22] As the particle size increases, the specific surface area decreases which limits the active sites on CDs.[15] Inhomogeneity in CD size can be avoided by adopting post-process filtering and dialysis. Also, gas chromatography, gel-electrophoresis, reversed phase chromatography or ion-exchange chromatography may be employed.[9]

2.2 Bottom-up approach

Here, CDs are obtained by carbonization of molecular precursors containing carbon, the required functional group and doping elements (Fig. 4a).[4] The bottom-up approach helps in achieving better structural and chemical homogeneity.[21,22] Some of the bottom-up synthesis routes are hydrothermal treatment, solvothermal method, pyrolysis, microwave pyrolysis/irradiation, *etc.* The microwave assisted reduction technique for CD synthesis has gained more attention recently since it provides homogeneous heating of the reaction mixture.[6] The main stages involved in this process are polymerization, dehydration and carbonization under microwave irradiation as illustrated in Fig. 4b. For instance, initially amine rich precursors form cross-linked clusters on polymerization which then undergo intermolecular and intramolecular dehydration to produce organic clusters with rich amine bonds. These are further carbonized to obtain carbon cores. The time and temperature of carbonization affect the optical properties of synthesized CDs.[4,6,14] Moreover, microwave treatment time influences the size of CDs with the formation of CDs of size 3–4 nm when treated for 5–20 min.[23] It is widely used as it is time and energy efficient and does not require complex equipment.[6,16] In hydrothermal treatment, the carbon precursor dissolved in water is converted to CDs in the presence of strong acids such as HNO_3, H_2SO_4 or H_2O_2 at high temperature and pressure to undergo dehydration followed by carbonization.[36,68] Acids in the reaction mixture introduce hydrophilic surface groups such as carbonyls, hydroxyls and carboxyls on the CDs.[69] It is a widely adopted CD synthesis method as it is eco-friendly, but requires high reaction temperature and time.[13,16] A wide variety of precursors such as citric acid,[36,49,52,68,69,71] urea,[4,68,70] polyamines[37] and biological precursors such as carbohydrates,[13,72] amino acids, lignin, mushroom,[4] polymers[73] *etc.*, were employed for CD synthesis through hydrothermal/microwave-assisted methods.[4] Furthermore, the soft template or hard template method where graphite like planar and highly symmetric molecules such as 1,3,5-triamino-2,4,6-trinitrobenzene (TATB) or hexa-peri-hexabenzo-coronene (HBC) were used as the carbon precursor and template was also reported.[2,12,13] Recently, microwave assisted hydrothermal treatment was developed to synthesize CDs in order to overcome the weakness of hydrothermal treatment. The mechanism of formation of GQDs by the microwave assisted hydrothermal treatment route is explained in Fig. 4c.[13]

In the solvothermal process, instead of water, different organic solvents such as ethanol, glycol, DMF, *etc.* are used. Solvents adopted for solvothermal processes affect the size

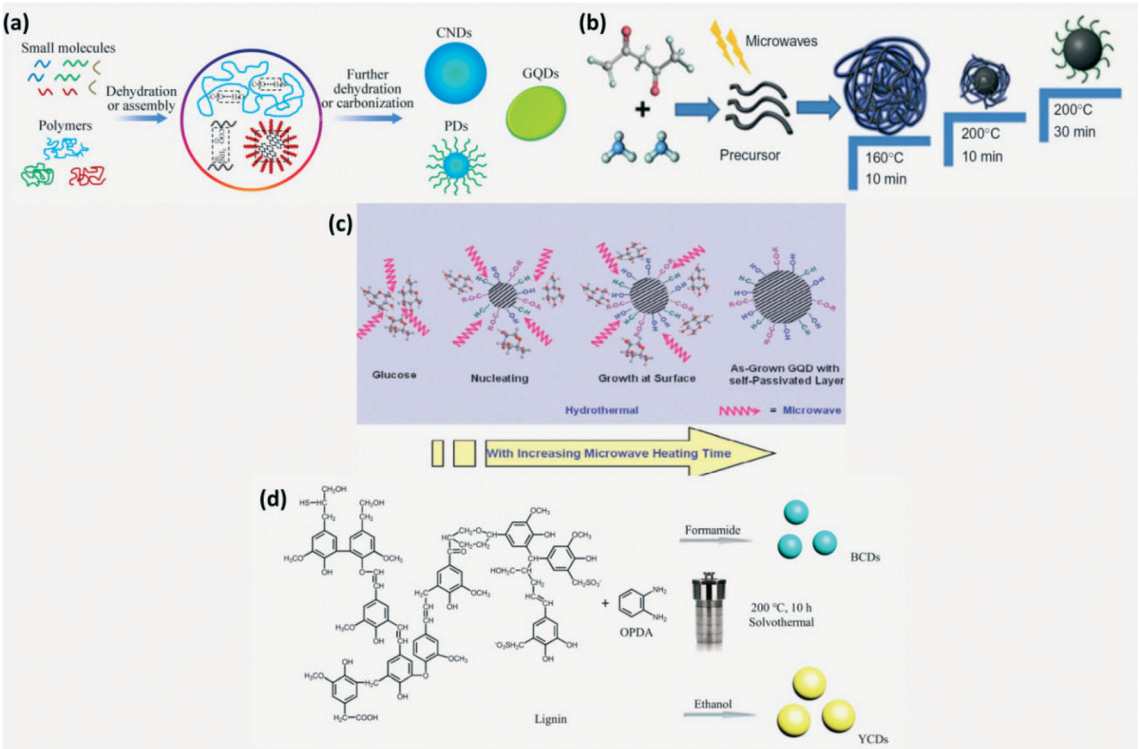

Fig. 4 (a) Schematic of the bottom-up approach.[13] Reproduced with permission from ref. 13, copyright, 2020, Royal Society of Chemistry. (b) Schematic of synthesis of N-CDs by microwave assisted reduction.[4,14] Reproduced with permission from ref. 4, copyright, 2019, Elsevier. (c) Schematic of the mechanism of formation of GQDs by the microwave assisted hydrothermal treatment.[13] Reproduced with permission from ref. 13, copyright, 2020, Royal Society of Chemistry. (d) Solvothermal synthesis of CDs from lignin in different solvents.[74] Reproduced with permission from ref. 74, copyright, 2020, American Chemical Society.

and surface state of CDs and hence their luminescence.[9] For instance, lignin and *o*-phenylenediamine dissolved in formamide and ethanol subjected to solvothermal treatment produced blue-CDs and yellow-CDs, respectively as shown in Fig. 4d. Solvothermal and hydrothermal synthesis routes have received more attention as high temperature and pressure are found to be conducive to the formation of conjugated graphite cores.[74] Amphiphilic CDs which are soluble in both polar and apolar media can be produced by the solvothermal technique.[5,29]

CDs have been grown by certain exotic routes such as confined reactions in nanoreactors, oxygen plasma treatment,[2] microplasma process,[10] *etc.* But the downside of the bottom-up synthesis approach is that these processes are complicated and the products obtained generally have poor solubility.[22]

2.3 Green synthesis

Several green methods to synthesize CDs have been developed recently in view of reducing environmental pollution and cost of production.[6,10,41,49,54] Green synthesis usually employs a bottom-up approach. It may be carried out using biomass such as protein, waste materials and organisms as raw materials or/and by sustainable synthesis techniques carried out at room temperature. Biomass-based CDs exhibit higher QY as they contain nitrogen.[6,75] But the CDs synthesized lack purity and homogeneity and their QY varies from batch to batch.[11,69] Since the QY of the CDs is not an important parameter for sensors, any source of raw material such as yogurt,[39] jackfruit,[76] bagasse,[72] bee pollen,[24] eggs,[6,24] fennel seeds,[11] ginger,[25] roasted gram peel,[49] saffron,[26] banana peel,[57,77] rice husk,[78] black sesame,[69] radish,[45] *etc.* can be used to synthesize CDs. Recently, several attempts have been made to produce CQDs on large scales with high yield using simple precursors.[24,36,40]

The precursors for CD synthesis must be chosen wisely as they affect the efficiency of the process, QY, surface energy, electronic structure and optical properties of the synthesized CDs. Moreover, for sensing application, the functional groups such as –COOH, –NH, –COH, *etc.* as well as doping elements such as N, S, Cl, B, P, *etc.* present on the CD surface play a major role in deciding their sensitivity and selectivity to a particular chemical compound and serve as chemically active sites for adsorption. These functional groups and doping conditions can easily be obtained by using amines, carbonyl, sulfonyl, alcohol containing organic, polymeric or/and biological compounds.[4,16] The size and chemical structure of synthesized CDs can be varied by controlling precisely the reaction parameters such as the precursor type, reaction time, temperature and solvents as they dictate the nucleation and growth conditions of CDs.[9,13,74] Small seed dots are formed initially which later grow to produce CDs through continuous carbonization at high temperature. As reaction

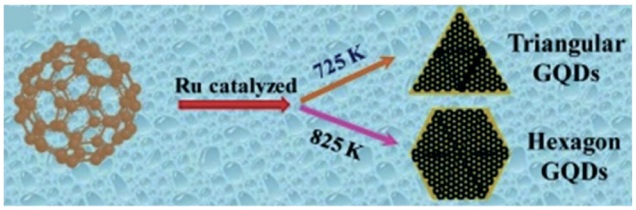

Fig. 5 Schematic of Ru-catalyzed C_{60} cage opening at different temperatures resulting in different GQD morphologies.[13] Reproduced with permission from ref. 13, copyright, 2020, Royal Society of Chemistry.

time increases, the amount of crystallinity in the carbon core increases.[6] Shape change with change in annealing temperature was observed in the case of the metal catalyzed C_{60} cage opening method for the synthesis of GQDs as shown in Fig. 5.[2,13] Carbon nanomaterials tend to agglomerate irreversibly due to strong π–π stacking or van der Waals forces in the absence of ions or a surfactant. This is prevented by surface modification through heteroatom doping and functionalization. The tendency of CDs to agglomerate or the extent of hydrophilicity can be determined by measuring their zeta potential. If the zeta potential is found to be in large negative or positive volts, then CDs stay dispersed else, they agglomerate.[25,39,45,69,79]

3. Sensing properties

Most of the observed properties of CDs can be modified by surface passivation. Varying CDs' size or the conjugate sp^2 domain size in the CD core results in varying band gap,

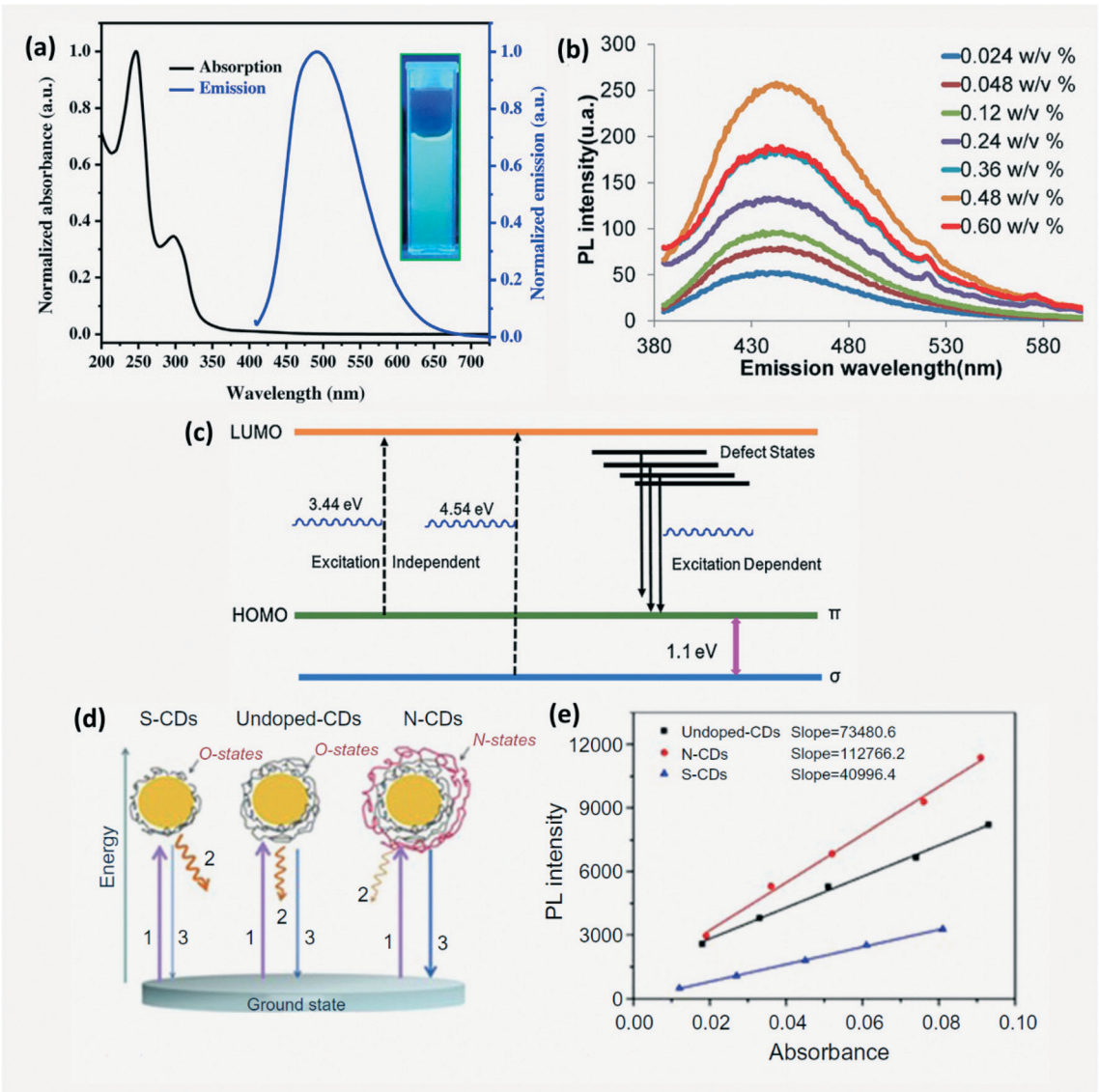

Fig. 6 (a) Absorption and emission spectra of CDs.[80] Reproduced with permission from ref. 80, copyright, 2016, Elsevier. (b) Agglomeration induced luminescence quenching of CDs.[82] Reproduced with permission from ref. 82, copyright, 2017, Elsevier. (c) Energy levels and electron transition for tunable PL emission from N,B-CQDs.[84] Reproduced with permission from ref. 84, copyright, 2019, Elsevier. (d) PL mechanism and (e) integrated PL intensity of S-CDs, undoped-CDs and N-CDs.[4] Reproduced with permission from ref. 13, copyright, 2019, Elsevier.

luminescence and electron transport ability.[9,18,19] Several specific functional groups or/and hetero-atoms present on the surface and edges of carbon dots serve as chemically active sites for adsorption of target molecules or formation of heterojunctions in composites.[9,39] Sorption of molecules at active sites may result in changed optical and electrical properties that are highly sought after for sensing applications.[30] The main optical and electrical properties of the CDs that can be exploited for the fabrication of gas sensors are explained in detail below.

3.1 Optical properties

In UV-vis absorption spectra of CDs (Fig. 6a), the wavelength peaks around 230–280 nm and 310–360 nm correspond to the π–π* transition of C–C bonds and the n–π* transition of C═O bonds, respectively.[2,15,39,41,80,81] The energy gap between π and π* orbitals depends on the size of sp^2 clusters or conjugation length.[2] CDs exhibit photoluminescence (PL), fluorescence (FL), chemiluminescence (CL), electrochemiluminescence (ECL), up-conversion photoluminescence and phosphorescence. Up-conversion PL is observed due to anti-Stokes PL emission where an electron excited from the π-orbital on relaxation returns to the σ-orbital.[2,29] CDs also exhibit excitation wavelength dependent emission where the emission is red-shifted with increasing excitation wavelength. This reveals the presence of a range of surface energy traps on CDs.[23,45] Amphiphilic CDs have been found to exhibit solvatochromism which is a phenomenon where the absorption and emission spectra have a strong dependence on the solvent polarity.[5,12] On aggregation of CDs in unsupported solid powder or solution, no luminescence is observed due to non-radiative internal conversion of excitons within CD energy traps and states as shown in Fig. 6b leading to agglomeration induced quenching.[30,39,82] Moreover, additional emission peaks may appear in the spectra of agglomerated CQDs due to deformation in molecular geometry which leads to formation of self-trapped states.[82] Thus, ensuring that CDs stay dispersed or immobilized is very important either using a surfactant or ions when dissolved in the liquid phase or by anchoring these on nanoparticles or polymer films/aerogel in the solid phase.[34,72,83]

3.1.1 Photoluminescence (PL). PL emission is classified into fluorescence and phosphorescence. These are observed due to the transition of an electron from the lowest unoccupied molecular orbital (LUMO) to the highest occupied molecular orbital (HOMO).[2] Although several researchers have proposed different mechanisms to explain the origin of PL based on experimental and theoretical work,[11] a universally accepted PL mechanism providing a satisfying explanation for the variation in PL wavelength with excitation wavelength, pH and synthesis conditions hasn't been proposed. Luminescence of CDs could be adjusted by deliberately controlling the condensation reaction, chemical manipulations, or by doping. Nitrogen (N), boron (B), sulfur (S) and phosphorus (P) are generally used as individual dopants or in combination to control PL spectral shift. Among these, nitrogen is the most commonly used dopant.[1,40] The PL properties vary with CD size, where small-sized CDs exhibit UV emission, medium-sized CDs demonstrate visible light emission, and large CDs exhibit near-infrared emission due to the quantum size effect.[1,9,15] The red shift in the PL peak is attributed to narrowing of the band gap by varying the functional groups and structural defects on the CD surface leading to radiative recombination of excitons.[9,41,45] The extent of emissive states appearing from the emission of the core and surface groups or the defects can be quantified from the full width at half maximum (FWHM) of the PL peak.[80] It has been suggested that emission at short wavelengths arises due to luminescence from the graphitic core, while deactivation pathways are responsible for emission at longer wavelength.[24] CDs synthesized by high energy methods have a good sp^2 conjugate core and hence facilitate the expression of intrinsic luminescence.[16] Excitation wavelength dependent emission was attributed to carbon cores, quantum confinement, surface states and dopants, while excitation independent PL was attributed to organic fluorophores, the degree of carbonization and shape.[10,11,24,26,37,47,69] In other words, excitation wavelength independent PL emission was proposed to occur due to n–σ* or n–π* transitions which necessitates a fixed amount of energy as shown in Fig. 6c.[84] It is proposed that the PL excitation independence can be controlled by tuning to a higher C═C/C═O to C–O–C/C–O peak ratio *i.e.* a lower degree of oxidation.[11] Complete carbonization of precursors is essential to obtain the maximum PL efficiency which can be controlled by varying the reaction temperature and time while using the disappearance of symmetric and asymmetric stretching peaks of CH_2 in FTIR of synthesized CDs as the checking point.[11,12]

QY (Φ) of CDs is calculated using

$$\Phi = \Phi_R \times \left(\frac{I}{I_R}\right) \times \left(\frac{A}{A_R}\right) \times \left(\frac{n^2}{{n_R}^2}\right) \quad (1)$$

where 'I' is the integrated emission intensity, 'A' is the absorbance measured by UV-vis spectroscopy, 'n' is the refractive index and R denotes the reference sample.[39,44,45,76] Usually quinine sulfate dissolved in 0.1 M sulfuric acid[10,26,73,78] or rhodamine B (ref. 13 and 59) is used as a reference. CDs with the highest QY are obtained in the presence of NH-functional groups. For instance, CDs produced by hydrothermal treatment of ethylenediamine and citric acid in an autoclave at 150–300 °C for 5 hours exhibit a 80% QY.[4,15,36] The order of QYs of citric acid derived CDs can be organized as N,S codoped-CDs > N-CDs > undoped-CDs > S-CDs. QY depends on the morphology of the CDs.[13] CPDs were reported to have higher QY than oxidized GQDs at high temperature.[12] Lu *et al.* proposed a simple mechanism to explain the variation in photoluminescence QY due to doping by considering undoped-CDs, N-doped CDs and S-doped CDs prepared as shown in Fig. 6d. The surface states of undoped CDs that were related to a wide range of energy levels were named O-states.[4,14] On N-doping, several additional surface states named N-states were added onto the CDs which resulted in higher QY,[4,14,42] whereas S-doped CDs exhibit lower QY due to partial elimination of O-states. Further, N,P

co-doped CDs were found to exhibit higher fluorescent emission and QY than only N or P doped CDs.[4,14]

In addition to this, pH and ionic strength in an aqueous environment can affect the PL. pH-Dependent PL has been investigated for CDs produced from jackfruit, to find that stable luminescence was observed for pH 3–11 while at very high or low pH, certain emissive states were destroyed.[76] At high pH, the negative charge density accumulated over the surface of CDs increases which in turn suppresses n–σ* or n–π* transitions responsible for independent PL emission which causes PL shift and emission intensity decreases. However, under highly acidic conditions, the blue shift of PL was observed due to proton adsorption on emissive sites. PL shift was also observed due to the solvent effect where surface passivation of CDs by solvent molecules or the electron withdrawing effect of doped atoms was the proposed cause.[39,84] Passivating the GQD surface with particular macromolecules like PEG was found to minimize PL variation and improve QY through higher quantum confinement of emissive states on their surface.[2]

3.1.2 Fluorescence (FL). CDs exhibit fluorescence with emission wavelength ranging from UV to near infrared. 3 main reasons for the origin of FL have been proposed over time: core-state emission, surface-state emission and molecular fluorescence.[6,53,85] Molecular state FL due to incorporation of small molecules or other impurities that serve as organic fluorophores is predominantly observed in CPDs as compared with other CDs. In addition to these, the cross-linked enhanced emission effect (CEE) also contributes to FL emission of CPDs wherein cross-linking suppresses the vibration and rotation of compounds which helps to reduce non-radiative relaxation. The dominance of a mechanism among these and the FL wavelength are determined by the extent of carbonization as shown in Fig. 7a. On increasing degree of carbonization,

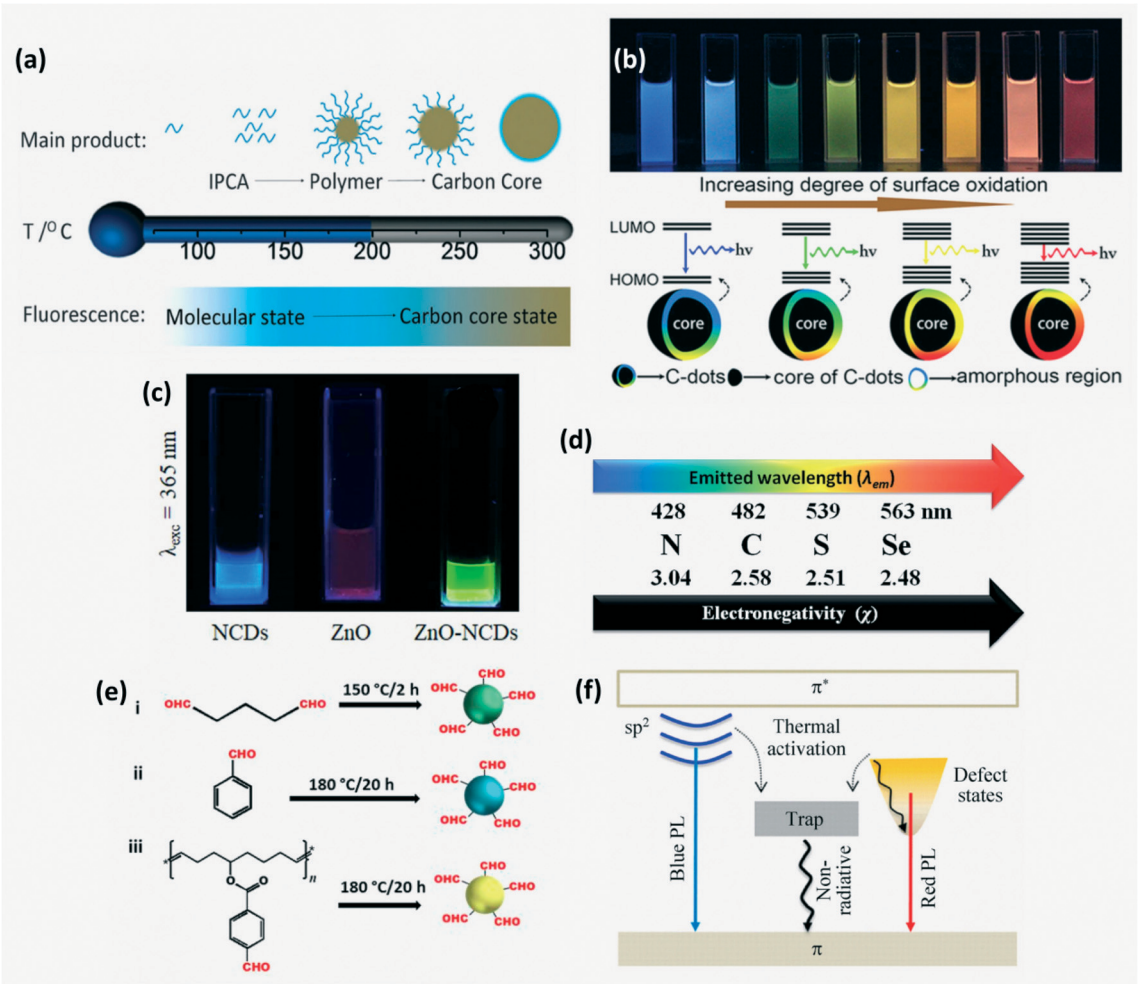

Fig. 7 (a) Variation in the dominant FL mechanism with CD synthesis temperature.[12] Reproduced with permission from ref. 12, copyright, 2019, Wiley-VCH. (b) Influence of the degree of surface oxidation on FL emission wavelength.[6] Reproduced with permission from ref. 6, copyright, 2019, Royal Society of Chemistry. (c) FL of aqueous solution of N-CDs, ZnO and ZnO/N-CDs hybrid under UV illumination.[70] Reproduced with permission from ref. 70, copyright, 2020, Frontiers. (d) Shift in emission wavelength with electronegativity of the dopant.[40] Reproduced with permission from ref. 40, copyright, 2014, Royal Society of Chemistry. (e) CDs exhibiting red, yellow and green FL on using different aldehydes as precursors.[34] Reproduced with permission from ref. 34, copyright, 2019, American Chemical Society. (f) Schematic of the optical behavior of GQDs resulting in different FL wavelengths.[85] Reproduced with permission from ref. 85, copyright, 2015, Springer.

carbonization-induced CEE increases which enhances the emission intensity and QY.[12,72,74,85] The surface state-based FL mechanism depends on the degree of surface oxidation. Increased surface oxidation gives rise to more surface defects which serve as trap centers to prevent radiative recombination. Moreover, the band gap of CDs decreases due to addition of new energy states resulting in red-shift of FL wavelength as shown in Fig. 7b. FL emission wavelength can be altered by varying the CD size, surface functional groups, heteroatom doping and degree of π-conjugation. Due to quantum confinement, FL emission gets red-shifted upon increasing the CD size. Doping CDs with N, P and S can increase QY through surface passivation.[6,16,29] It was found that the lower the electronegativity of doped atoms, the higher the emission wavelength and the lower the QY (Fig. 7d). FL behavior can be controlled further by varying these dopant concentrations. For instance, adding sulfur atoms as dopants on CDs can influence the total amount of oxygen based functional groups and hence on increasing S concentration the FL is red shifted. Further, CDs have a very short FL lifetime of a few nanoseconds and this lifetime is dependent on heteroatom doping with heavy doped CDs having a longer FL lifetime.[6,40] Although it is difficult to synthesize CDs with long FL wavelengths, in recent years CDs that fluoresce with orange[81] or red emission[72,77] have been successfully synthesized for application in optical-electronic based sensors. Red or orange emissions are attributed to large particle size and high N content which results in larger conjugated sp^2 domains.[74,77] Long wavelength luminescence was also possible on relaxation of electrons excited by π–π* transition through a defect state.[85]

Moreover, the FL of CDs when grafted onto a metal oxide or polymer is different from when they are dispersed freely in water. For instance, silica aerogel-PEI capped CQDs exhibit 30 nm blue shift in FL wavelength as compared to CQDs in aqueous solution due to strong electrostatic interaction between the negatively charged silica surfaces and the positively charged PEI on the surface of the CQDs.[86] In CD grafted ZnO-pSi, electrons transfer to the LUMO of N-CD on excitation and emit green luminescence on relaxation as opposed to blue FL by bare N-CDs as shown in Fig. 7c.[70] Among –N, R–NH and $–NH_2$ groups, –N has the highest positive impact, while among the –SH, –SR and ═S groups, –SH has the highest positive impact on the optical performance of CDs. It has been found that if both RNH and –SH groups exist in the precursors, then the best optical performance is observed due to the formation of small fluorophore molecules –NH–C–C–SH on the CD surface.[4] Researchers have reported that the type of carbon precursor used for CD synthesis also influences the FL wavelength. For example, an aliphatic dialdehyde – glutaraldehyde yielded green-FL CDs, an aromatic aldehyde – benzaldehyde produced blue-FL CDs and a cyclooctadiene–aldehyde based polymeric derivative yielded yellow CDs as depicted in Fig. 7e.[34]

3.1.3 Phosphorescence. Room temperature phosphorescence (RTP) involves intersystem crossing of electrons with a change in their spin multiplicity during transition from the triple excited state to the ground state with a large time delay. C═O/C═N groups in CDs were proposed to be RTP origin sites and the higher the degree of graphitization of synthesized CDs, the lower the RTP lifetime due to destruction of these origin sites.[2,74] The mechanism of RTP and its difference compared to FL is explained in Fig. 8. It helps in obtaining better visual signals since background emission and light scattering can be avoided.

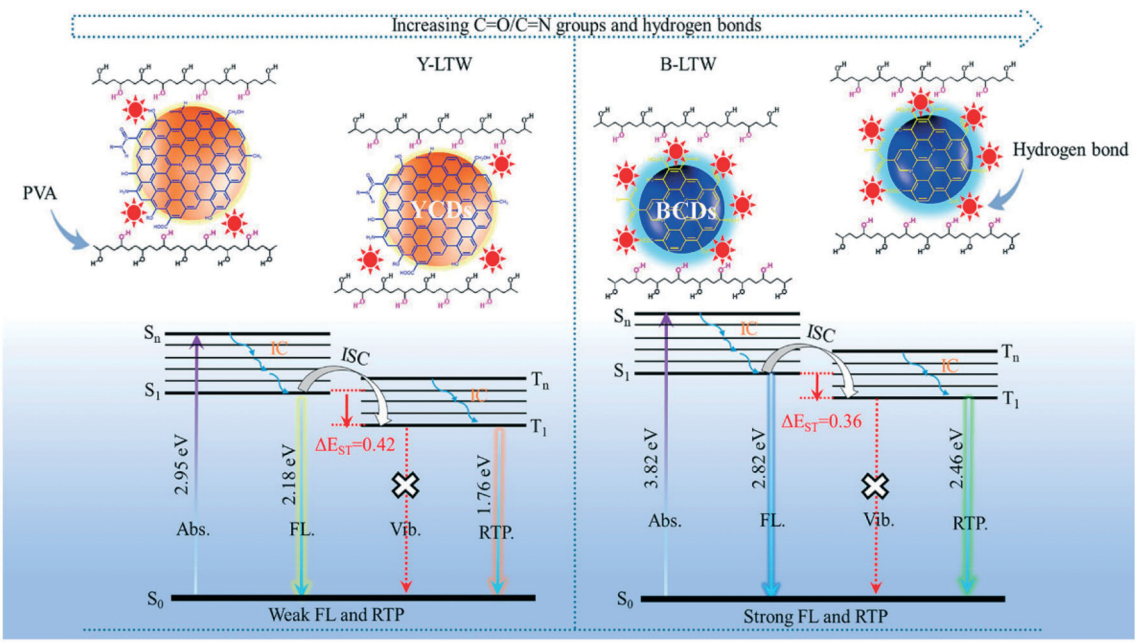

Fig. 8 Schematic explaining FL and RTP emission of Y-CDs and B-CDs.[74] Reproduced with permission from ref. 74, copyright, 2020, American Chemical Society.

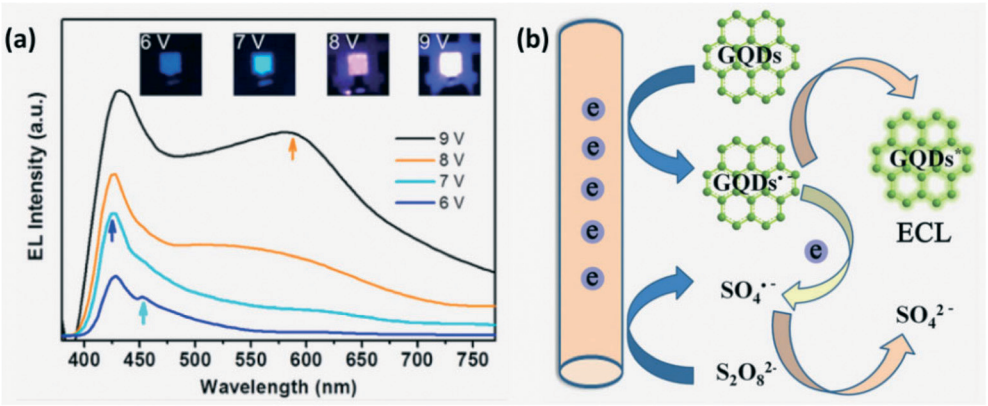

Fig. 9 (a) Switchable ECL of CDs for different working voltages.[31] Reproduced with permission from ref. 31, copyright, 2013, American Chemical Society. (b) Simple schematic illustrating the ECL mechanism in GQDs.[8] Reproduced with permission from ref. 8, copyright, 2012, Wiley-VCH.

Liu *et al.*[74] observed RTP in blue CDs (B-CDs) where on irradiation n–π* excitation of N and O doped-CDs occurs initially and on relaxation, the electron undergoes an intersystem crossing from the singlet excited state to the triplet excited state. Strong hydrogen bonds formed between the transparent wood (TW) and B-CDs resulting in a dense structure that provides a good oxygen barrier which helps to stabilize the triplet excitons when CDs are grafted on TW. Thus, excitons possess a very long decay lifetime resulting in delayed emissions.

3.1.4 Chemiluminescence (CL). CL refers to luminescence produced from a chemical reaction. It is hypothesized that the energy separations for CD surface states responsible for CL emissions are smaller as compared to those responsible for PL. Studies indicate that CDs exhibit CL emission only when they interact with oxidants strong enough to oxidize the singlet orbital of the CDs. CL emission can also be caused by electron–hole annihilation or radiative recombination of electron injected and hole injected CDs.[23]

3.1.5 Electrochemiluminescence (ECL). Electrochemiluminescence is a type of luminescence where the electrochemical energy is converted into radiative energy.[13] Zhang *et al.*[31] demonstrated switchable ECL of CDs with color varying from blue to white for different working voltages or more precisely, different injection current densities favoring recombination with different decay times as shown in Fig. 9a. For lower injected charge density, energy levels associated with faster recombination and decay pathways are chosen. It was observed that the white ECL emission spectra included the co-existence of different color emission peaks due to multiple recombination processes occurring at very high current density.[15,31]

Several mechanisms have been put forth to explain ECL in CDs. Two models proposed by researchers that are widely accepted are band gap emission of the conjugated π-domain and the edge effect due to surface defects.[15] Li *et al.*[8] explained that the ECL mechanism involves the formation of highly oxidizing radicals (SO_4^{2-}) and GQD radicals initially. Upon transfer of an electron between these radicals, an excited molecule GQD* is generated which on returning to its ground state emits light as illustrated in Fig. 9b. Green luminescent-GQDs inherit the high content of sp^2 carbon domains from graphene and this along with the difference in energy gap accelerates electron transport during the ECL process.[29]

3.2 Electrical properties

CDs can behave as p-type or n-type semiconductors depending on the doping elements or functional group. It was observed that the pH of the precursor solution can influence the electrical resistance of the GQDs obtained. Moreover, zigzag GQDs are metallic where zigzag sites are carbene-like, while armchair GQDs are semiconducting where armchair sites are carbyne-like.[19,85] Generally, CDs have a very large surface area, more active sites for molecule adsorption, and high conductivity which help in rapid charge transfer. On utilizing CDs in conjunction with other p/n-type materials, a p–p, n–n or p–n nano heterojunction can form successfully which improves charge transfer across the nanocomposite. For instance, a GQD–SnO_2 co-modified ZnO gas sensor exhibits better response, sensitivity and high charge mobility due to the formation of an n–p–n heterojunction with p-type GQDs and n-type ZnO and SnO_2

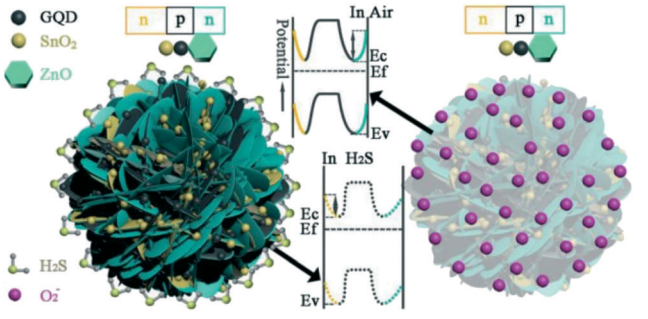

Fig. 10 Schematic of the band configuration at the hetero-junction interface of GQD–SnO_2/ZnO nanostructure on exposure to air and H_2S.[87] Reproduced with permission from ref. 87, copyright, 2020, American Chemical Society.

nanoparticles as shown in Fig. 10. Further, the junction barrier potential can be controlled by doping, adding functional groups or adsorption of target molecules. Doping GQDs with N leads to minute distortion since the atomic size of nitrogen and carbon is similar, a positive shift in the Fermi level and an increase in basicity.[65,87] CDs can be used as electrochemical sensors which are further classified as potentiometric, amperometric and conductometric based on the type of electrical signal measured.[13,61]

4. Classification of gas sensors based on the sensing mechanism

Briefly, CD-based gas sensors can be classified into fluorometric, mass-based and chemiresistive sensors depending on whether the optical or electrical properties of CDs are adopted for sensor signal and response measurement.

4.1 Optical sensors (fluorometric)

Optical sensors have certain advantages over electrical sensors as they are not affected by electromagnetic interference, do not pose a risk as an ignition source during volatile organic compound (VOC) leakage, and have high efficiency and a wide area of coverage.[30,76] Polarity, interfacial energy and electronic coupling of VOCs and CDs were found to be the main parameters which affect the electronic state that influences the optical properties of CDs. Gas molecules having larger dipole moments induce a larger effect on the energy band gap of these CQDs. Several computational studies have been carried out to identify the reactive sites and explain different interactions occurring between the target gas molecules and CDs.[76,78] Changes occurring in the energy gap and HOMO and LUMO levels of CDs during adsorption of a target molecule were studied.[49,88] But optical sensors may suffer from drift in the final signal depending on the loading of fluorophores into the sensor system which affects their reproducibility.[82] Modulation of different optical properties of CDs is adopted as a sensor signal. Some of the methods used for sensing gas molecules are discussed briefly here.

4.1.1 Increased optical absorbance. Thongsai *et al.*[78] reported that the absorbance of CQDs on exposure to different VOCs increased with increasing polarity, while the emissivity decreased as shown in Fig. 11a and the order of the measured absorbance value for various VOCs was water >

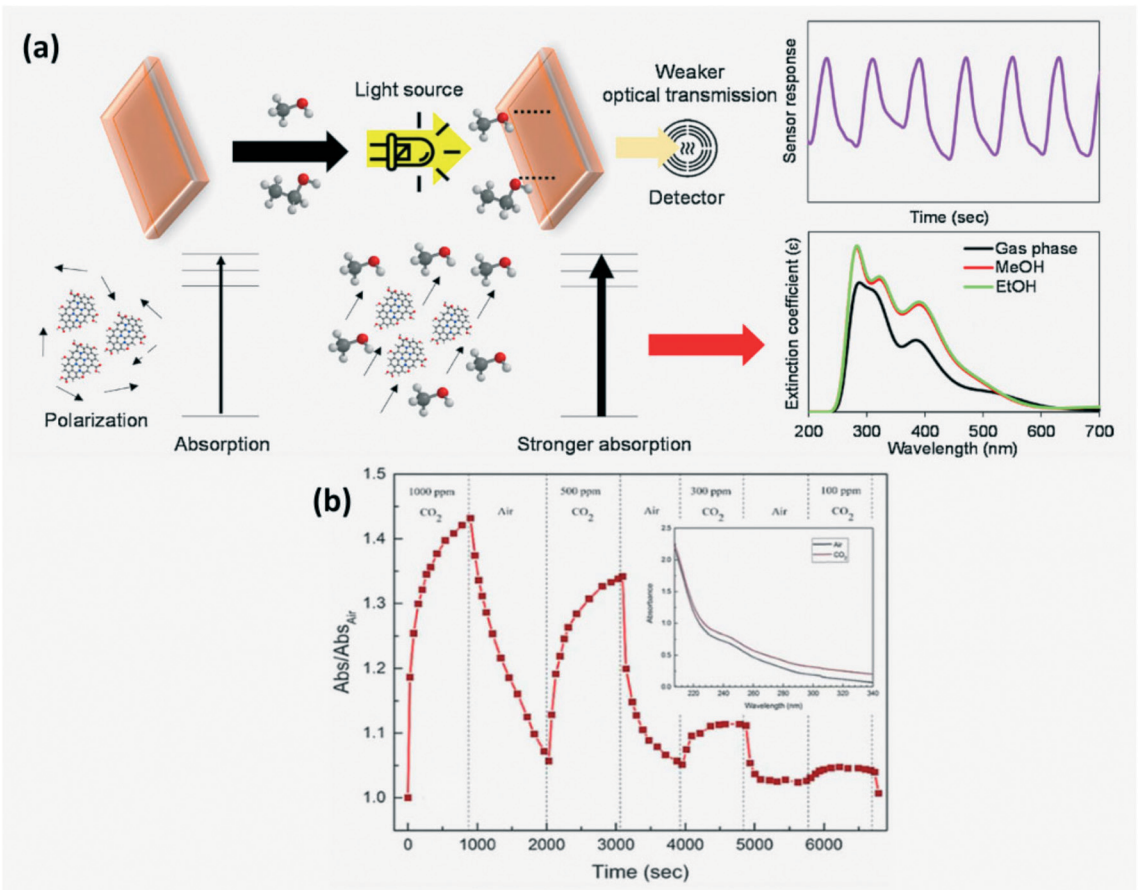

Fig. 11 (a) Schematic diagram of modulation of optical absorbance of CDs and their response curve on exposure to solvent.[78] Reproduced with permission from ref. 78, copyright, 2019, Elsevier. (b) Response curve of GQDs for detecting CO_2 gas at 310 nm.[30] Reproduced with permission from ref. 30, copyright, 2020, Institute of Physics.

methanol > diethyl ether > dichloromethane > hexane. GQD sensors have been utilized to detect CO_2 with an average response time of 106 s and recovery time of 150 s, wherein on adsorption of CO_2 on the GQD surface, CO_2 bonds on the basal plane and edge of GQDs increase, thus increasing the optical absorption intensity as seen in Fig. 11b.[30]

4.1.2 Fluorescence (FL) quenching (turn-off). FL quenching can be briefly classified into (i) dynamic quenching involving diffusion related interaction or collision between the CDs and quencher leading to a charge or energy transfer and (ii) static quenching involving non-fluorescent complex molecule formation between the ground CDs and quencher.[14,38,41,84] In addition to this, FL quenching can take place on adsorption of certain chemicals on CDs in conjunction with metal oxides or mesoporous materials by the inner filter effect (IFE) and photoinduced electron transfer (PET). The energy gap between the LUMO of an electron donor and the HOMO of an electron acceptor is the driving force for PET and it is further classified into reductive PET and oxidative PET depending on whether CDs act as electron donors or receptors, respectively. Some of the energy transfer mechanisms that may occur during FL quenching are fluorescence resonance energy transfer (FRET), surface energy transfer and Dexter energy transfer. FRET involves photonic energy transfer between 2 fluorophores with spectral overlap and DET involves electron transfer between 2 molecules with matching redox potential. An overlap of emission and excitation wavelengths of CDs with the absorption spectrum of the quencher can lead to IFE. If no change in fluorescence lifetime is observed during FL quenching, then IFE is the involved FL quenching mechanism.[6,14,17,38,41,46,47,53,81,89] The dynamic quenching kinetics follows the Stern–Volmer relation of

$$\frac{F}{F_0} = 1 + k_q \tau_0 [C] \quad (2)$$

where 'F' and 'F_0' are the FL intensity of CDs in the presence and absence of a quencher, k_q is the quench rate, τ_0 is the FL

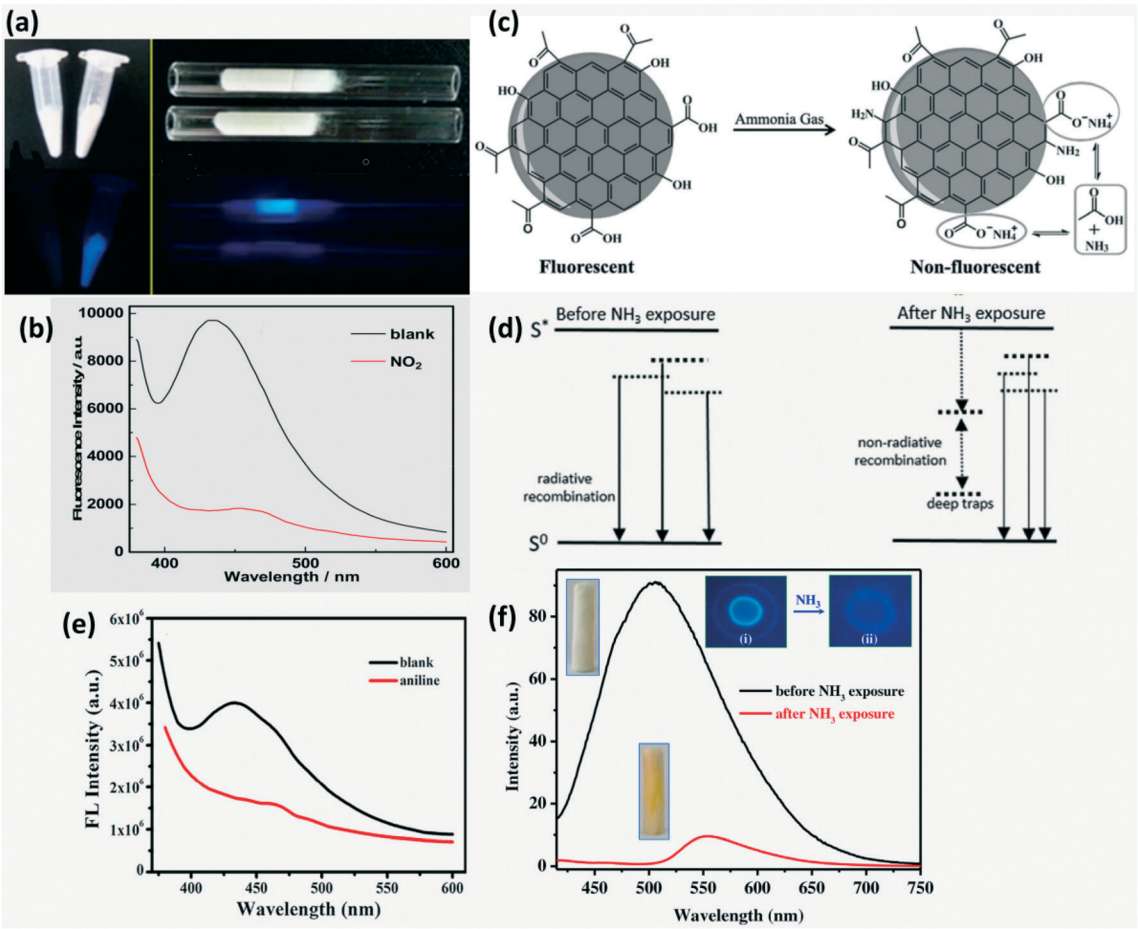

Fig. 12 (a) Digital image of CDs and CDs-aerogel in the presence and absence of NO_2 vapors; (b) FL quenching of aerogel-CDs by aniline vapors.[86] Reproduced with permission from ref. 86, copyright, 2013, American Chemical Society. (c) Illustration of NH_3 sensing by PVDF-RCDs.[72] Reproduced with permission from ref. 72, copyright, 2015, Wiley-VCH. (d) Energy state of the CDs in the presence and absence of NH_3 with additional traps causing FL quenching in the presence of NH_3.[73] Reproduced with permission from ref. 73, copyright, 2017, Elsevier. (e) FL Quenching of aerogel-CDs by aniline vapors.[83] Reproduced with permission from ref. 83, copyright, 2019, Elsevier. (f) FL Spectra of the CD rhodizonate sensor before and after NH_3 vapour exposure (300 ppm), (i) and (ii) image of the dried sensor solution on the silica plate before and after NH_3 exposure, respectively.[80] Reproduced with permission from ref. 80, copyright, 2016, Elsevier.

lifetime and [C] is the quencher concentration.[38,47] The higher the electron donating ability of a gas molecule and the lower the steric hindrance, the higher the extent of FL quenching in the CD sensors.[90]

Silica aerogel-PEI capped CQDs exhibit reversible adsorption of NO_2 and hence were tested for detecting NO_2 gas with high sensitivity and selectivity. Strong FL quenching (Fig. 12a and b) by NO_2 was hypothesized to be from the interaction of electron-withdrawing NO_2 and electron-donating PEI on the CQD surface which impedes the radiative recombination of electrons and holes trapped on the CQD surface.[86] Similarly, Ma *et al.*[83] reported a silica aerogel/CQDs based composite for sensing aniline gas through FL quenching (Fig. 12e) due to electron absorption by the CQD composite from electron donating aniline which suppresses the radiative recombination of electrons and holes.

A strong FL quenching of red-CQDs coated on PVDF film by NH_3 gas was proposed to occur in two steps namely irreversible and reversible adsorption of NH_3 molecules on the surface as shown in Fig. 12c. Ammonia induced Michael addition consists of irreversible addition of N into C=C finally forming C–N which results in irreversible quenching. In reversible quenching, deprotonation of the carboxyl group occurs (–COOH + NH_3 = $–COO^-$ + NH_4^+) due to acid–base neutralization.[72] S-doped CQDs based on the same mechanism of FL quenching by ammonium salt formation and change in surface acidity were developed by researchers to sense NH_3 through a reaction between ammonia and sulfonic/carboxylic acid on the S-CQD surface. In addition to this, they proposed that (i) amine formation through the reaction of ammonia with phenols, cyclic ethers or diketones, (ii) amide formation through the reaction of ammonia with C=O of carboxyl groups/acid anhydrides and (iii) Michael's addition can also lead to FL quenching. These newly formed surface functional groups serve as traps enhancing non-radiative recombination (FL quenching) as shown in Fig. 12d.[73] Desorption of ammonia can be driven by depositing a CD-based sensor material on hydrophobic fibers.[82]

Förster (fluorescence) resonance energy transfer (FRET) based "on–off" sensors can be used to detect several chemicals such as pesticides,[53,91] immunoglobulin,[48] ammonia,[80,82] *etc.* by combining the fluorescent probe with a nanomaterial-based quencher. The FRET process is achieved when an electron donor and an acceptor separated by a distance of <10 nm have sufficient spectral overlap in the absorption spectra of the electron acceptor and the emission spectra of the electron donor. Energy transfer between these molecules occurs through non-radiative dipole–dipole coupling or electrostatic interaction due to opposite charges on their surfaces.[6,38,41,44,80,82] Such a phenomenon occurred on exposing the CDs-sodium rhodizonate(II) hybrid to NH_3. Addition of sodium rhodizonate(I) to CDs functionalized with COOH groups causes protonation and subsequent dehydration which results in colorless rhodizonate dihydrate form (II) (Fig. 12f). On exposure to NH_3, FL quenching of CDs is observed due to deprotonation of rhodizonate(II) (dual role – recognizer and quencher/fluorophore) to rhodizonate(I) whose spectra overlap with CDs. This leads to a red shift. Ultra-fast energy transfer occurs from CDs to rhodizonate(I) since exchange of the virtual photon in energy transfer is a kinetically fast process.[38,80] Meanwhile in the case of the CDs-fluorescein based FRET complex sensor prepared by Hsu and coworkers,[82] NH_3 detection was due to reversible imine bond formation between ammonia and ketones on CDs or carboxylic groups on fluorescein assisting in energy transfer. The FRET efficiency of the CD based complex is measured as

$$E = 1 - \frac{I_{DA}}{I_D} = 1 - \frac{\tau_D}{\tau_{DA}} \quad (3)$$

where I_{DA} and I_D are the integrated emission peak of CDs in the composite in the presence and in the absence of a FRET acceptor, respectively, while τ is the FL lifetime.[38,82]

On exposure to formic acid vapor, the FL intensity of CQDs reduces which is used as the sensor signal.[39] Similarly, a CQD produced from a green method was used for detection of several polar VOCs by measuring the changes in CQD absorbance and emissivity. A change in FL emissivity of CQDs on exposure to VOCs is hypothesized to be due to hydrogen bonding and polar–polar interaction between VOC molecules and CQDs or change in polarization around the CQDs by solvent molecules.[78] Mesoporous silica microspheres (MSM) and hollow mesoporous silica microspheres (HMSM) doped with CDs and mesoporous silica sieve with a uniform hexagonal pores (SBA-15) in conjunction with varied concentration of CDs that fill in the pores and ordered internal channel were developed to detect oxygen quantitatively and qualitatively by observing the amount of FL quenching of the compound as shown in Fig. 13a. CDs are locked onto the pores of MSMs and the ordered structure of mesoporous carriers improves gas diffusion effectively. CD-HMSMs have higher quenching response than CD-MSMs due to their higher crystallinity and specific surface area, ordered cylindrical pores in the shell and larger pore volume for flow of target gas molecules but had a longer response and recovery time compared to CD-MSMs.[92] Luminescence quenching of (7%) CDs/SBA-15 in homogeneous media exhibited a non-linear dependence due to different adsorption sites as shown in Fig. 13b and is explained by several models.[75] Yang *et al.*[93] fabricated a highly sensitive and selective sensor containing amino-CQDs encapsulated in sulfo-modified metal organic frameworks (MOF) (MIL-101-SO_3H) for detection of dinitrophenol (DNP) in air. Here FL quenching occurred due to an overlap in the emission peak of immobilized amino-CQDs with the absorption peak of DNP adsorbed on the pore surface MIL-101-SO_3H and charge transfer. A simple, highly sensitive and selective aerogel produced from cellulose was grafted with PEI passivated CDs to develop a nitric oxide sensor where CDs served 3 purposes namely as a rigid cross-linking agent, as an adsorption site and as an FL probe. The bright blue FL of the sensor was quenched on exposure to nitric oxide (NO_x) because of electron transfer from electron donating PEI to electron withdrawing NO_x preventing radiative recombination.[52]

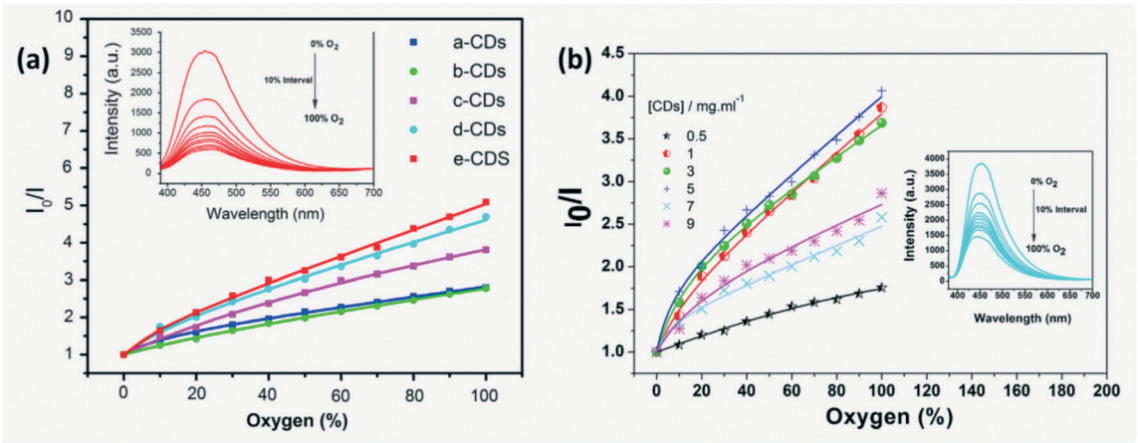

Fig. 13 (a) FL quenching observed on exposure to O_2 through luminescence intensity plots for 5% CD assembled samples ((a-CDs) 5% CDs-SMSMs, (b-CDs) 5% CDs-CMSMs, (c-CDs) 5% CDs-TMSMs, (d-CDs) 5% CDs-CHMSMs and (e-CDs) 5% CDs-THMSMs).[92] Reproduced with permission from ref. 92, copyright, 2016, Elsevier. (b) Luminescence intensity plots for CDs-SBA15 samples.[75] Reproduced with permission from ref. 75, copyright, 2016, Elsevier.

4.1.3 Fluorescence restoration (turn-on). N-CQDs with surface decorated Ag nanoparticles (NPs) through Ag–N bond formation were developed as H_2S sensors where FRET based FL quenching was observed initially due to energy transfer between Ag NPs and N-CQDs. On exposure to H_2S, AgCQD + H_2S → HCQD +AgHS reaction occurs due to which the Ag–N bond is replaced by a stronger Ag–S bond and some of the Ag NPs are released from the N-CQD surface thus restoring CQD fluorescence as shown in Fig. 14a.[94]

4.1.4 Fluorescence enhancement. An MCM-41/CQD based mesoporous fluorescence sensor was produced to detect acetic acid both in solution and vapor phase. The sensor was more sensitive to acetic acid vapors than its solution. In addition to an increase in FL intensity, a slight red-shift in emission wavelength occurs on exposure to acetic acid. But the increase in FL intensity on exposure to acetic acid alone was used as the sensor signal.[71] Supchocksoonthorn *et al.*[69] developed a CD-based ammonia sensor whose FL intensity increases with incremental NH_3 concentration both in solution and vapor phase. Addition of nitrogen on the CD surface through NH_3 adsorption and polar–polar interaction between hydrophilic groups on the CD surface and NH_3 was reported to be the cause for enhanced emissivity. Praneerad *et al.*[45] reported that on exposure to acetic acid, CD absorbance decreased while emissivity increased due to polar interaction between gas molecules and CDs as shown in Fig. 14b.

4.1.5 Shift in PL or FL peak. A shift in the PL or FL peak is observed when CDs are localized close to electron donors. For instance, the CD-silica aerogel-based gas sensor developed to detect aromatic VOCs exhibits spectral shift along with luminescence quenching as shown in Fig. 15a. In addition, the amount of observed wavelength shift for other VOCs has been compared in Fig. 15b.[90] Another VOC sensor composed of N,B-doped CQDs/PVA film was fabricated by Liu *et al.*[84] to detect acetone vapors by observing a PL shift from blue green to blue in air with a simultaneous increase in PL intensity as shown in Fig. 15c. Amphiphilic CDs which fluoresce with different wavelengths for different VOCs as shown in Fig. 15d were developed to detect precisely several VOCs.[5]

4.1.6 Ratiometric fluorescence sensors. CD-based sensors working on ratiometric fluorescence are usually used for biosensing but recently they have been adopted for gas

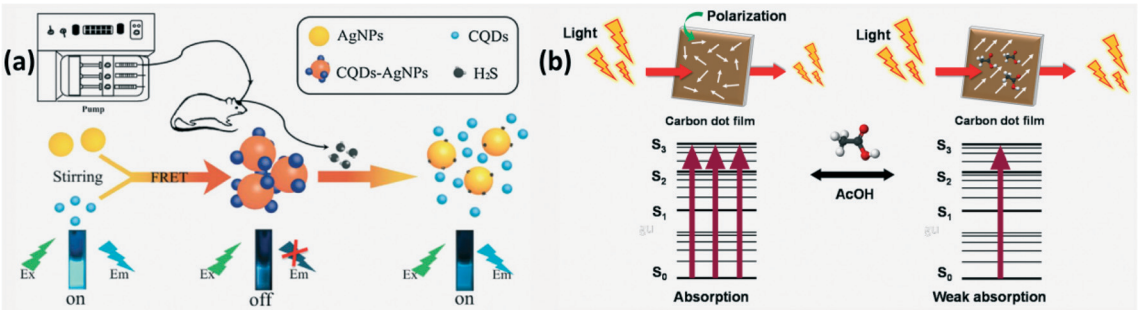

Fig. 14 (a) Illustration of the FL turn-on mechanism of the CQDs-AgNPs nanoprobe by H_2S.[94] Reproduced with permission from ref. 94, copyright, 2018, Elsevier. (b) Schematic of modulation of optical absorbance of CDs in the presence and absence of acetone.[45] Reproduced with permission from ref. 45, copyright, 2019, Elsevier.

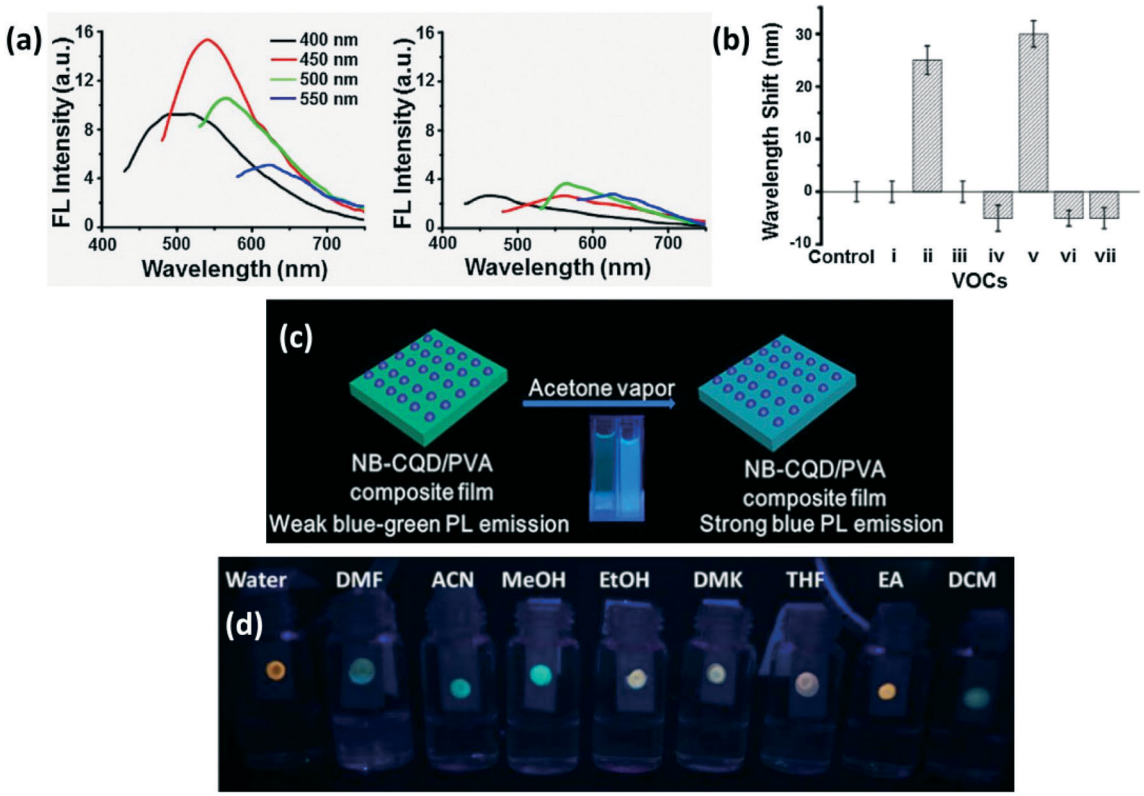

Fig. 15 (a) Excitation dependent FL spectra of CDs-aerogel in the (i) presence and (ii) absence of aniline vapors; (b) extent of the FL peak shift in the presence of different VOCs (i. benzene; ii. aniline; iii. *o*-phenylenediamine; iv. *m*-phenylenediamine; v. *p*-phenylenediamine; vi. nitrobenzene; vii. phenol).[90] Reproduced with permission from ref. 90, copyright, 2017, Elsevier. (c) Schematic of acetone vapor detection by N,B-CDs by PL shift.[84] Reproduced with permission from ref. 84, copyright, 2019, Elsevier. (d) Digital photo of CDs absorbed in paper strip showing different types of luminescence in different solvents.[5] Reproduced with permission from ref. 5, copyright, 2016, Royal Society of Chemistry.

sensing. Such sensors have gained more attention as they can be monitored by visual inspection and easily calibrated to apt accuracy using references unlike single FL intensity dependent sensors. They may involve an energy transfer between two types of fluorophores with spectral overlap, *i.e.* the emission wavelength of one of the fluorophores is in the vicinity of the excitation wavelength of other fluorophores.[41,46,74,77] He *et al.*[77] developed a blue luminescent CD (B-CD) and red luminescent CD (R-CD) co-doped mesoporous alumina (MA) that exhibited ratiometric fluorescence in the presence of oxygen. Its mechanism is similar to FRET and the energy transfer efficiency can be calculated using

$$\eta = 1 - \frac{\tau_{\text{B-CD/R-CD}}}{\tau_{\text{B-CD}}} \quad (4)$$

where $\tau_{\text{B-CD}}$ and $\tau_{\text{B-CD/R-CD}}$ are the decay lifetime of B-CD single doped and B-CD/R-CD/MA, respectively.[77] In dual-CDs synthesized for formaldehyde (FA) sensing, yellow CDs (Y-CDs) were more sensitive to FA since the O-containing surface groups on CD were able to react with reducing gas FA and accept its electrons while in blue CDs (B-CDs), electron rich N-containing groups prevented FA adsorption. Thus, on FA adsorption, the $I_{\text{B-CD}}/I_{\text{Y-CD}}$ value is reduced.[74]

4.1.7 Chemiluminescence (CL). CL-based CD sensors are preferred over electrochemical detection as they have high sensitivity, low background interference and simplicity.[23,29] CL detection of nitrites has been carried out in gaseous as well as aqueous phases. Gaseous phase detection involves reduction of nitrites to NO and their subsequent reaction with ozone to form electronically excited NO_2^* that emits light on returning to its ground state. For liquid phase detection, peroxy nitrous acid (ONOOH) forms by mixing H_2O_2 with nitrites. Oxidants, ONOOH and OH* act as hole injectors producing R^{+}* while oxygen radicals act as electron injectors producing R^{-}* (R refers to CDs). The CL mechanism was explained by interaction of hole injected (R^{+}*) and electron injected (R^{-}*) CDs resulting in radiative electron–hole annihilation as shown in Fig. 16. Furthermore, ONOOH transfers energy to CDs since excited ONOOH* releases light at 350–450 nm which overlaps with the excitation spectra of CDs which partially accounts for the observed CL from CDs.[23]

4.1.8 Room temperature phosphorescence (RTP). An on-site real time responsive building material was developed by Liu *et al.* to detect an indoor pollutant, formaldehyde (FA). The blue CD grafted luminescent transparent wood (B-LTW@Cr(VI)) based sensor showed RTP quenching and restoration in the absence and presence of formaldehyde,

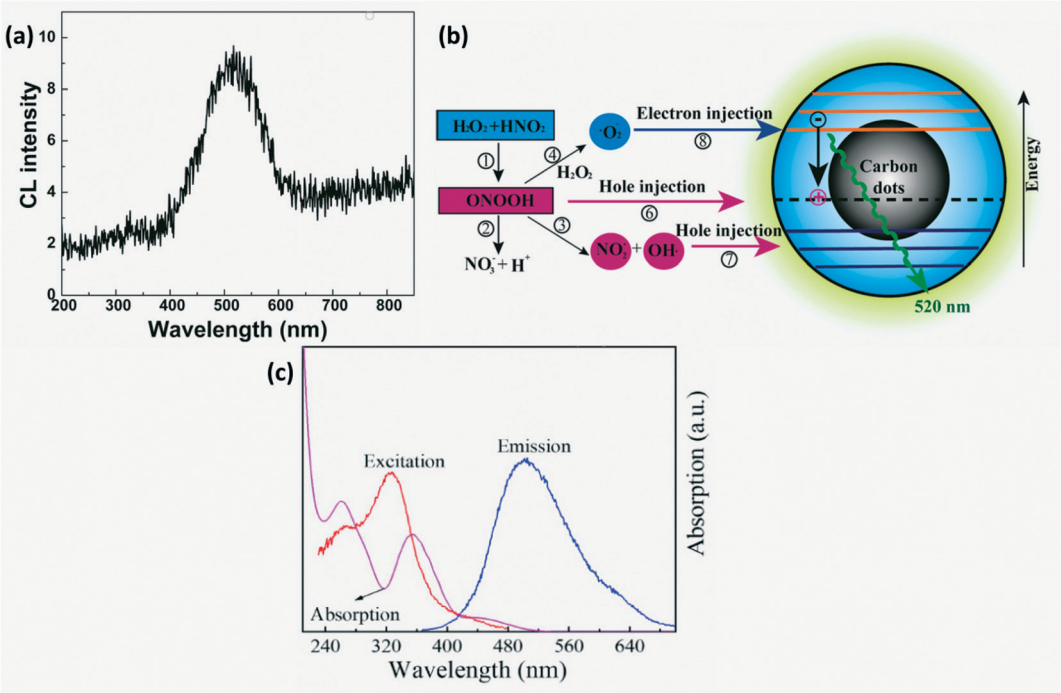

Fig. 16 (a) CL spectra and (b) schematic of the CL mechanism in CDs-$NaNO_2$–H_2O_2.[23] Reproduced with permission from ref. 23, copyright, 2011, American Chemical Society. (c) Absorption spectra of Cr(VI), RTP excitation & emission spectra of B-LTW.[74] Reproduced with permission from ref. 74, copyright, 2020, American Chemical Society.

respectively. On addition of Cr(VI) to B-CDs, RTP quenching was observed due to IFE wherein the excitation spectra of B-CDs and absorption spectra of Cr(VI) overlapped as shown in Fig. 16c. On exposure to FA, Cr(VI) was reduced to Cr(III) restoring the RTP of B-CDs.[74]

4.1.9 Dye formation. CDs were synthesized as solution phase sensors to detect the NO level in water and cells as NO serves as an indicator of inflammation due to severe damage in living cells. One of the NO detection routes (Fig. 17a) involves the reaction between NO and alkyl amine on CDs producing a nitroso-amine intermediate which results in a diazonium ion which finally generates molecular nitrogen. Another route involves a diazo-coupling reaction to form a diazo-dye-conjugated CD network that serves as the signal.[95]

4.2 Quartz crystal microbalance

A quartz crystal microbalance consists of a thin quartz wafer whose vibration frequency varies with variation in its mass per unit area or thickness. But a pristine quartz crystal does not have sufficient sensitivity. To overcome these limitations, GQDs prepared from pyrolysis of citric acid were uniformly deposited on thin quartz wafer to selectively and sensitively detect acetone vapors as shown in Fig. 17b. On exposure to acetone, gas molecules are physisorbed/chemisorbed on the GQD surface through van der Waals interaction of gas molecules and hydroxyl, carboxyl and carbonyl groups on CDs and through a percolation–diffusion process. Since GQDs possess a large surface area,

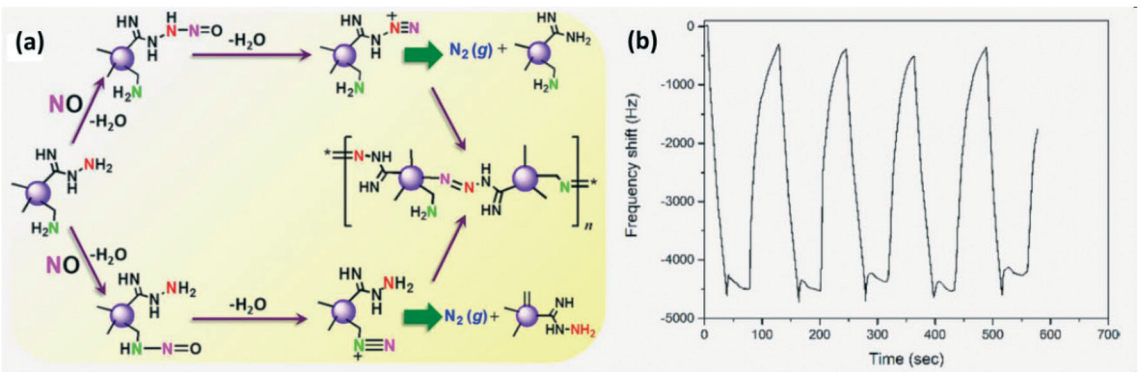

Fig. 17 (a) NO detection mechanism of CDs to form azo-dye.[95] Reproduced with permission from ref. 95, copyright, 2017, American Chemical Society. (b) Response–recovery cycle of a GQD-based QCM gas sensor.[22] Reproduced with permission from ref. 22, copyright, 2021, MYU K.K.

more acetone molecules may be adsorbed which results in improved sensitivity sensors.[22]

4.3 Chemiresistors

Chemiresistors measure the change in sensor resistance on adsorption or desorption of gas molecules from the sensor surface through interaction between surface functional groups and target gas molecules. Adsorption of oxidizing gases like NO_2, CO_2 or SO_2 decreases resistance (increases conductance), while adsorption of reducing gases such as NH_3 or H_2S increases resistance of p-type semiconductors (MOs or CDs).[27] The reverse is true for n-type. The response of the conductometric sensor is provided by

$$S(\%) = \frac{\Delta R}{R} \times 100 \quad (5)$$

where $\Delta R = R_{gas} - R_0$, R_{gas} and R_0 are the resistance of the sensor on exposure to gas and pure air, respectively.[61,67,68]

Commonly used resistive elements are semiconductor metal oxides (MOs) such as WO_3, Co_3O_4, ZnO, Sn_2O_3, Fe_2O_3, *etc.* whose electrical properties can be modified by doping to obtain tailored sensor response.[66,96,97] But the downside is that they possess poor selectivity and have to be operated at high temperatures to enhance response and recovery, as well as surface adsorption which requires to overcome certain energy barriers and consumes a considerable amount of power. This is because at high temperature, more electrons are available to react with oxygen molecules in ambient air and adsorb abundant oxygen on their surface which reacts with the target gas leading to a resistance change.[18–20,60,65,66,97,98] Also, at high temperature, grains coarsen and the surface area reduces which in turn reduces sensor response.[98,99] Although metal oxide nanoparticles can be surface imprinted with organic molecules to improve the selectivity and response of sensors against molecules with structural similarity, the mobility of charge is low and the resistance is high due to introduction of these organic molecules. Hence, the required operating temperature will still be high.[20] Furthermore, few MOs such as ZnO and SnO_2 are susceptible to base or acid degradation.[76] Generally, n-type MOs are widely used since they have higher stability and compatibility. However, recently p-type MOs have been explored due to their good catalytic activity towards reducing gases and high O_2 solubility, thus a rapid recovery.[61,98] Conducting polymers such as poly(3,4-ethylenedioxythiophene)-poly(styrenesulfonate) (PEDOT-PSS) and polyaniline (PANI) have also been investigated as sensor films but they suffer from poor response, poor thermal stability and swelling upon adsorption of gas molecules leading to increased resistance.[68,69,97,100] Thus, it is imperative to develop a resistive gas sensor operating at room temperature with high stability, sensitivity and selectivity, short response and recovery time and good reproducibility and reversibility.

CD-based resistive gas sensors can operate at room temperature and their gas sensing mechanism is generally attributed to the adsorption or desorption of target molecules on the active sites of the CD sensor. These adsorbed species may act as donors or acceptors, leading to a change in the HUMO or LUMO level of CDs, which alters the energy gap (E_{gap}) and thus changes the resistance/conductivity of CDs (GQDs or CQDs). Thus, they are simple to fabricate and show lower power consumption.[19,27,66,101] The bond energy of bonds formed during adsorption of target gas molecules on CDs is very important in determining the sensitivity of the sensor.[51] The main factors which improve gas sensing response in CD-composites is improved conductivity through the formation of nano heterojunctions, a high surface area and chemically active sites for sorption.[102]

Surface functionalization of CDs is the best approach to improve selectivity. Moreover, CDs can be doped with B to form p-type, while N, S or Cl doped CDs act as n-type semiconductors. Successful doping can be confirmed by Raman spectra for each type of doped GQD as shown in Fig. 18a and b wherein boron (low electronegativity) stiffens the Raman spectra frequency and causes red shift, while S, N and Cl (high electronegativity) soften the Raman scattering frequency resulting in blue shift.[27,41,84] In the case of N-GQDs, the dominance of graphitic N results in n-type semiconductor behavior, while the dominance of pyrrolic and pyridinic N on edges and defects of GQDs results in p-type.[99] Furthermore, GQDs exposed to gases at different pH levels were found to exhibit different resistance behaviors *i.e.* in neutral pH, GQDs behave as p-type.[19] Theoretical as well as experimental work has been carried out to study the interaction, charge transfer between the dopant on GQDs and gas molecule and variation in the binding energy of the target gas molecule to GQD and its band gap.[101] Nanoscale engineering of p–p, n–n, and p–n heterojunctions with carbon-based materials (carbon nanotubes, graphene, graphene oxide, CDs) and MOs is an effective method to improve sensor response at room temperature.[67,98] Such a nano heterojunction serves as a carrier reservoir. The presence of carboxyl groups on the CD surface infuses a large quantity of oxygen into the lattice of MO which serve as active sites for adsorption and chemical reaction. The Schottky barrier is formed at the p–n junction of CDs with MOs or conducting polymers which may be forward or reverse biased during their operation as a sensor. It was reported that the variation in the potential barrier height due to gas adsorption will lead to variation in their resistance.[87] The number of CDs used in conjunction with MOs or polymers is also important since too low concentration of CDs will lead to negligible changes in sensor sensitivity compared to the pure material, while too high a concentration of CQDs will result in a very small resistance change in air and target gas since charge conduction by CDs is very high.[103] In addition to this, CDs can also act as dopants for modification of the electronic structure of hierarchical compounds.[104]

In addition to the sensor material, the choice of electrodes is important in chemiresistors. For instance, Hakimi *et al.*[105] investigated the difference in the sensor

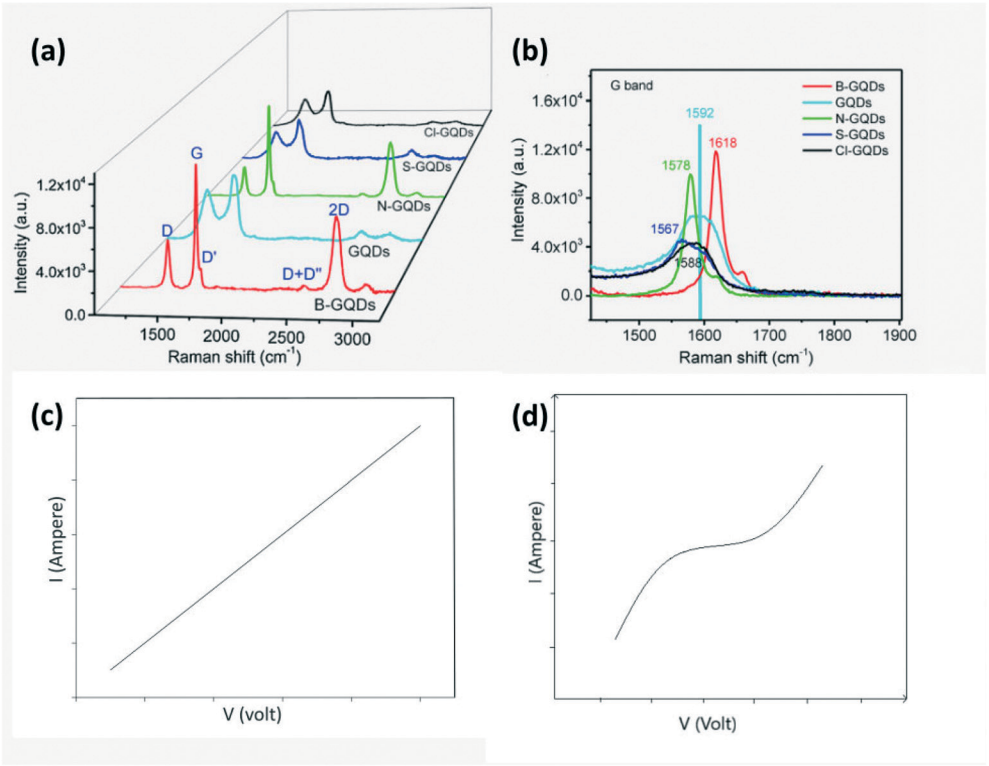

Fig. 18 (a) Raman spectra of GQDs, B-GQDs, N-GQDs, S-GQDs, Cl-GQDs; (b) amplified of view of (a).[27] Reproduced with permission from ref. 27, copyright, 2018, Elsevier. (c) *I–V* measurements of N-GQDs/PANI sensors with Ag electrodes and (d) Al electrodes.[105] Adopted from ref. 105, IEEE.

response on using Ag or Al as an electrode. The Ag-electrode showed ohmic behavior, while the Al-electrode showed Schottky behavior as observed from the *V–I* diagram (Fig. 18c). Schottky behavior was observed due to the presence of a potential barrier at the interface between the conducting polymer and Al. Meanwhile if the work function of the electrode metal is closer to the Fermi level of the sensor film, it would result in ohmic contact. If an electrode forms a Schottky junction, the position of the electrode with respect to the sensor film will also affect the performance since both bulk and junction resistance will contribute to sensor reading.

4.3.1 p-Type. In p-type materials, adsorption of oxygen on the surface on exposure to atmosphere captures electrons from the sensor, thus decreasing its resistance.[4,20,27] Adsorbed oxygen species are generally molecular ions at low temperature and atomic ions at higher temperature formed by the following reactions.[79,98–100]

$$O_2(\text{air}) = O_2(\text{ads}) \quad T < 100\ ^\circ\text{C} \tag{6}$$

$$O_2(\text{ads}) + e^- = O_2^-(\text{ads}) \quad \text{for } 100\ ^\circ\text{C} < T < 300\ ^\circ\text{C} \tag{7}$$

$$O_2^-(\text{ads}) + e^- = O_2^{2-} \leftrightarrow 2O^-(\text{ads}) \quad \text{for } T > 300\ ^\circ\text{C} \tag{8}$$

The order of ability of adsorbed oxygen to return the electron depending on its adsorbed state is $O_2 < O_2^- < O^- < O^{2-}$.[51] Now on exposure to reducing gases, electrons are injected back to the conduction band which combines with the majority carriers of p-type, reduces the hole density and makes the hole accumulation layer thinner while the depletion layer increases which leads to increased resistance.[19,20,27] Meanwhile on exposure to oxidizing/electron accepting gases, the target gas molecules replace the adsorbed oxygen species which results in an influx of holes and hence the resistance decreases with the increase in the majority charge carrier density.[79]

A flexible sensor was fabricated from N-doped or S, N-codoped CQDs/conducting polymers through a simple process as depicted in Fig. 19a.[68] Conducting polymers such as PANI and PEDOT-PSS behave as p-type semiconductors with the chemisorbed oxygen or H^+ (from dissociated water molecules in air) increasing the conductivity and exposure to a reducing gas will increase their resistivity. For instance, on exposure to NH_3, the following reactions will take place

$$4NH_3 + 5O^{2-} \rightarrow 4NO + 6H_2O + 5e^- \tag{9}$$

$$\text{G/PANI-H}^+ + NH_3 \rightarrow \text{G/PANI} + NH_4^+ \tag{10}$$

which injects electrons into the conduction band, thus increasing the depletion layer and resistance. But the initial adsorption of O_2 onto the polymer surface is very low at room temperature which would degrade its performance and this can be improved by increasing the temperature. However, on

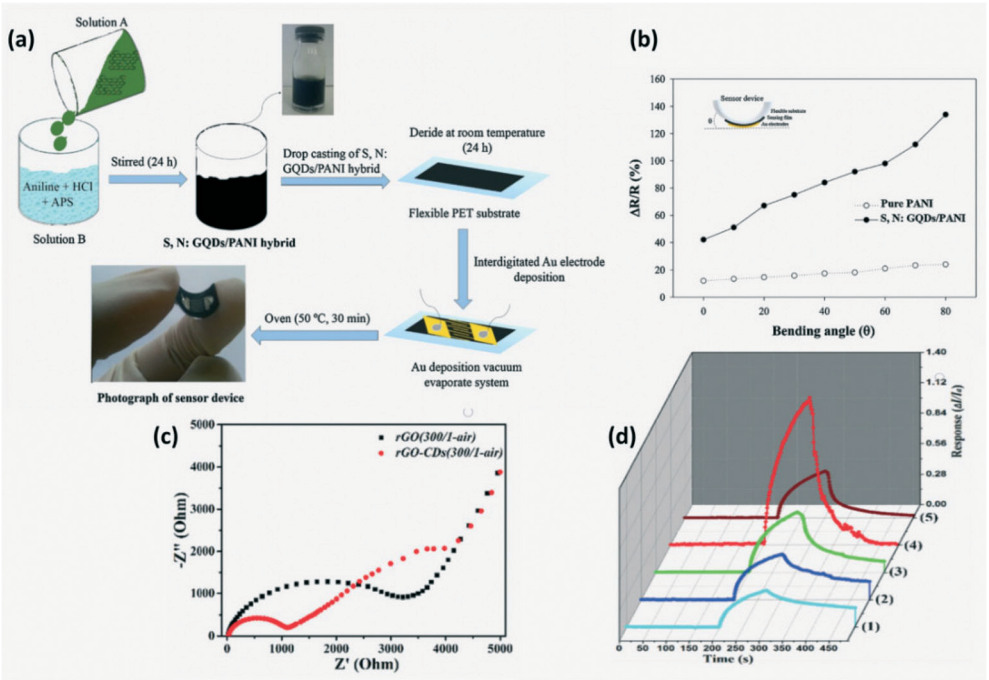

Fig. 19 (a) Synthesis route of flexible N,S codoped-GQDs/PANI sensors; (b) effect of flexibility on gas response of pure PANI and N,S-GQDs/PANI hybrid gas sensors on exposure to 100 ppm NH_3 at 25 °C in 57% relative humidity.[68] Reproduced with permission from ref. 68, copyright, 2016, Elsevier. (c) EIS plots of rGO (300/air) and rGO–CDs (300/air); (d) response cycle of (1) rGO, (2) rGO (300/air), (3) rGO–CDs, (4) rGO–CDs (300/air) and (5) rGO–CDs (300/N_2) to 50 ppm NO_2.[79] Reproduced with permission from ref. 79, copyright, 2017, Royal Society of Chemistry.

increasing the working temperature of sensors, their sensitivity reduces since adsorption of NH_3 is exothermic. Instead, on combining with N-GQDs, a p–n heterojunction is formed and the charge transfer and response of PEDOT-PSS/N-GQDs improve due to increased active sites and faster conducting pathways.[68,100,105] Further, an increase in sensor response was observed with increasing bending angle of these flexible sensors as seen in Fig. 19b.[68]

Using CDs in conjunction with MOs, aerogel or hydrogel has been verified to provide a resistive sensor film with higher sensitivity, selectivity and stability. Although several reduced graphene oxide (rGO)–MO based heterostructures were designed earlier for gas sensing, they had unsuitable band gaps and poor uniformity. *In situ* incorporation of CDs to rGO increases the hole density and lowers the Fermi energy levels of rGO nanosheets by forming heterojunctions through amide linking. NO_2, a strong electron acceptor, gets selectively adsorbed at grain boundaries or heterojunctions of rGO–CDs (p-type) or reacts with adsorbed oxygen species as shown in reactions (11)–(13). rGO–CDs show improved sensitivity towards NO_2 gas (~120%) with a shorter response and recovery time in comparison to bare rGO or rGO–MO due to similar crystal lattice parameters and improved charge transmission across the all-carbon nanoscale heterojunction (Fig. 19d). Electrochemical impedance spectroscopy (EIS) plots proved that the charge transfer resistance of rGO–CD hybrid < rGO as observed in the Nyquist plot (smaller semicircle = lower impedance) (Fig. 19c).[79]

$$NO_2\,(gas) + e^- = NO_2^-\,(ads) \quad (11)$$

$$NO_2\,(gas) + O_2^-\,(ads) + 2e^- = NO_2^-\,(ads) + 2O^-\,(ads) \quad (12)$$

$$NO_2^-\,(ads) + 2O^-\,(ads) + 2e^- = NO_2\,(gas) + 2O^{2-}\,(ads) \quad (13)$$

GQD/MQDs were developed to detect NO_2/NH_3 where MQDs (MoS_2 based quantum dots) containing structural sites can serve as gas adsorption sites or as dopants temporarily, while GQDs serve as conducting pathways. GQDs act as p-type semiconductors and depending on whether the adsorbed gas is reducing (NH_3) or oxidizing (NO_2), the resistance of the sensor decreases or increases accordingly as shown in Fig. 20a. Due to high binding energy, desorption of the target gas is difficult and hence the recovery time of the sensor is high. The recovery time and sensitivity were balanced by carefully controlling the temperature of the sensor through direct heat or photothermal heating.[106] Unlike the above hybrid CD-based sensor films which require stringent synthesis conditions, Sawalha *et al.*[107] fabricated a pristine carbon dot-based conductometric sensor film to detect minute concentration of NO_2. The O^- decorated CD film acts as a p-type semiconductor whose resistance decreases on adsorption of NO_2 since NO_2 extracts electrons, increases majority charge carrier hole density and thus reduces the Schottky barrier height.

B-GQDs serve as p-type semiconductors and on combining these with $AgLaFeO_3$(AL) which is another p-type perovskite semiconductor, the operating temperature was reduced and

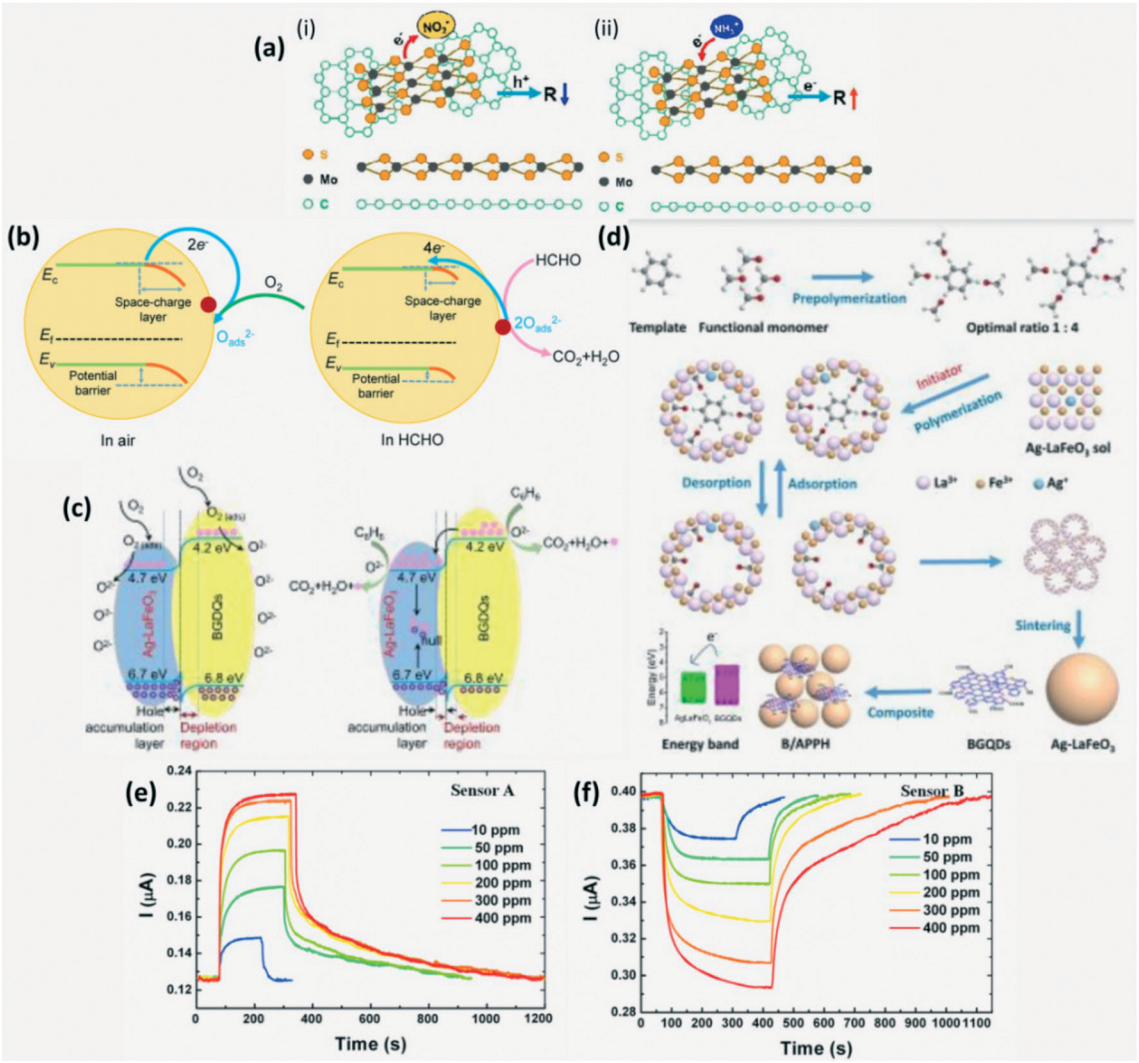

Fig. 20 (a) Schematic illustration of the mechanism of (i) NO_2 and (ii) NH_3 sensing respectively.[106] Reproduced with permission from ref. 106, copyright, 2016, Royal Society of Chemistry. (b) Schematic illustration of the charge transfer mechanism in sensors on exposure to HCHO.[27] Reproduced with permission from ref. 27, copyright, 2018, Elsevier. (c) Schematic illustration of the gas sensing mechanism of BI-AL in air and in benzene; (d) schematic of the BI-AL synthesis process.[20] Reproduced with permission from ref. 20, copyright, 2018, Royal Society of Chemistry. (e) Acidic-GQDs sensor response curve; (f) neutral-GQDs sensor response curve for different concentrations of NH_3.[19] Reproduced with permission from ref. 19, copyright, 2016, Elsevier.

the performance of sensors to selectively detect FA was further increased. As explained in Fig. 20b, adsorption of HCHO injects electrons into the energy band of B-GQDs (4.2 eV) which serve as a band bridge between AL (4.7 eV) and HCHO (3.9 eV).[27] Improved sensitivity and response to reducing gas such as benzene over structurally similar xylene and toluene was achieved by molecular imprinting on AL nanoparticles to obtain BI-AL with recognition cavities complementary to benzene molecules and finally grafting it with B-GQDs for lower operating temperature as shown in Fig. 20d. The detection mechanism is explained in Fig. 20c.[20]

Neutral GQDs are considered to be p-type and adsorption of NH_3 containing a lone pair of electrons increases their resistance through reduced hole density (Fig. 20f). COOH on acidic-GQD tends to ionize to COO^- and thus NH_3 is adsorbed and forms NH_4^+ which increases surface ion conductivity (Fig. 20e).[19] A metal phthalocyanine–GQDs (MPc–GQDs) based NO_2 sensor was developed with high selectivity and sensitivity where MPc serves as a p-type semiconductor, while GQDs enhance the conductivity by providing rapid charge transfer. On adsorption of NO_2 which is an electron withdrawing gas, the density of majority charge carriers (holes) on MPc–GQDs increases which results in reduced resistance and upon desorption, their resistance reverts to a higher value. The NO_2 desorption and adsorption rate was increased by laser irradiation on the sensor material.[66]

4.3.2 n-Type. In n-type MOs, atmospheric oxygen would get adsorbed on the surface and get ionized. This traps the electrons in the conduction band, further increasing the resistance and forms a layer of chemisorbed oxygen species. Similarly, N-doped or S-doped or Cl-doped CDs serve as

n-type semiconductors whose resistance increases on adsorption of oxygen species. On adsorption of oxidizing gas, their resistance increases due to further decrease in the electron density in the conduction band, while on adsorption of reducing gas, their resistance decreases due to influx of electrons.[27,67,102,104] Addition of CDs to mesoporous MOs helps in enhancing gas adsorption and charge transfer.[98]

The excellent NO_2 sensing (Fig. 21b) by the In_2O_3/CDs hybrid was attributed to the electron transfer across the heterojunction between In_2O_3 (4 eV) and CDs (5.56 eV), and the availability of more active sites for sorption of gas molecules due to the introduction of CDs. The NO_2 sensing mechanism of In_2O_3/CD hybrids is explained in Fig. 21a. The heterojunction formed at the interface of CDs and In_2O_3 increases O_S (surface adsorption oxygen) and O_V (oxygen vacancy) concentration which serve as adsorption sites. Addition of CDs improved the selectivity of the sensor towards NO_2 as compared to pristine In_2O_3 (which shows almost the same order of response for NO_2 and methanol) (Fig. 21c).[104]

Although single wall carbon nanotubes (SWCNTs) are expected to behave as p-type, on heavily doping with electron rich CDs, the SWCNT/CDs composite behaves as an n-type semiconductor. Since SWCNTs are hollow, upon introducing CDs on their surface, an electron accumulation layer forms over the wall of SWCNTs. On exposure to NO_2, the electrons in the conduction band are transferred from the sensor surface to NO_2 causing band bending upwards which results in increased resistance as shown in Fig. 22a and b.[97] N-GQDs in conjunction with SnO_2 were developed to detect NO_2 with higher sensitivity and selectivity due to a large surface area, active sites and rapid electron transfer across the GQD–SnO_2 hetero-interface. A Schottky barrier forms at the interface of N-GQDs and SnO_2 due to the difference in their energy levels/work functions. An increase in sensor resistance was observed on adsorption of electrophilic NO_2 suggesting that N-GQD/SnO_2 served as an n-type semiconductor with widening of the depletion layer in the presence of oxidizing gas as shown in Fig. 22c. The effect of temperature on the response of N-GQD/SnO_2 as opposed to that of pristine-SnO_2 is shown in Fig. 22d suggesting an improved performance at room temperature.[65]

A ZnO–GQD based sensor was developed for sensing ammonia since the heterojunction formed by ZnO and GQDs can serve as an adsorption site for gas molecules. The sensor has high selectivity and sensitivity as shown in Fig. 23B. On application of a strong electrostatic field, physisorbed H_2O molecules dissociate to produce hydronium and hydroxide ions where OH^- binds with Zn^{2+} while H_3O^+ further decomposes to give water molecules and highly conductive H^+ ions with a high diffusion coefficient. These H^+ ions move freely over the surface resulting in proton hopping. On exposure to NH_3 vapor, these ions react spontaneously to form NH_4^+ ions, dropping further the sensor resistance. The

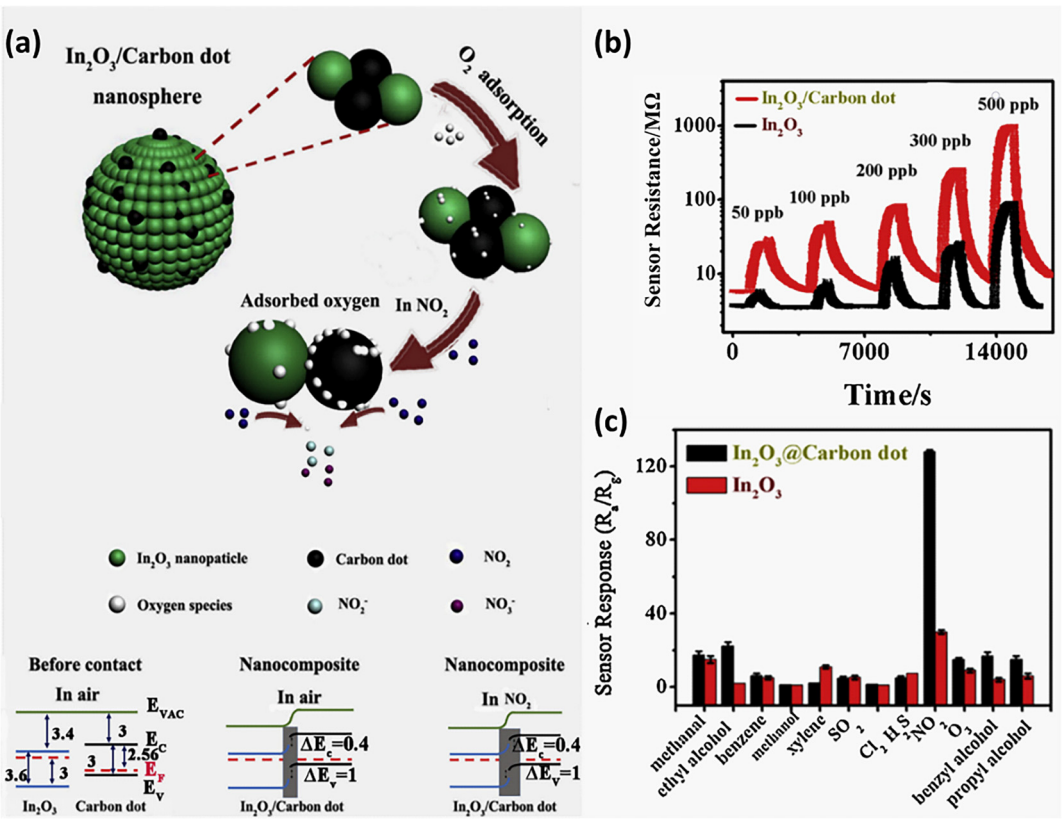

Fig. 21 (a) Schematic of the sensing mechanism of In_2O_3/CD hybrids to NO_2; (b) response cycle of In_2O_3/CDs to NO_2; (c) selective detection of NO_2 by In_2O_3/CDs as compared to In_2O_3 sensors.[104] Reproduced with permission from ref. 104, copyright, 2020, Elsevier.

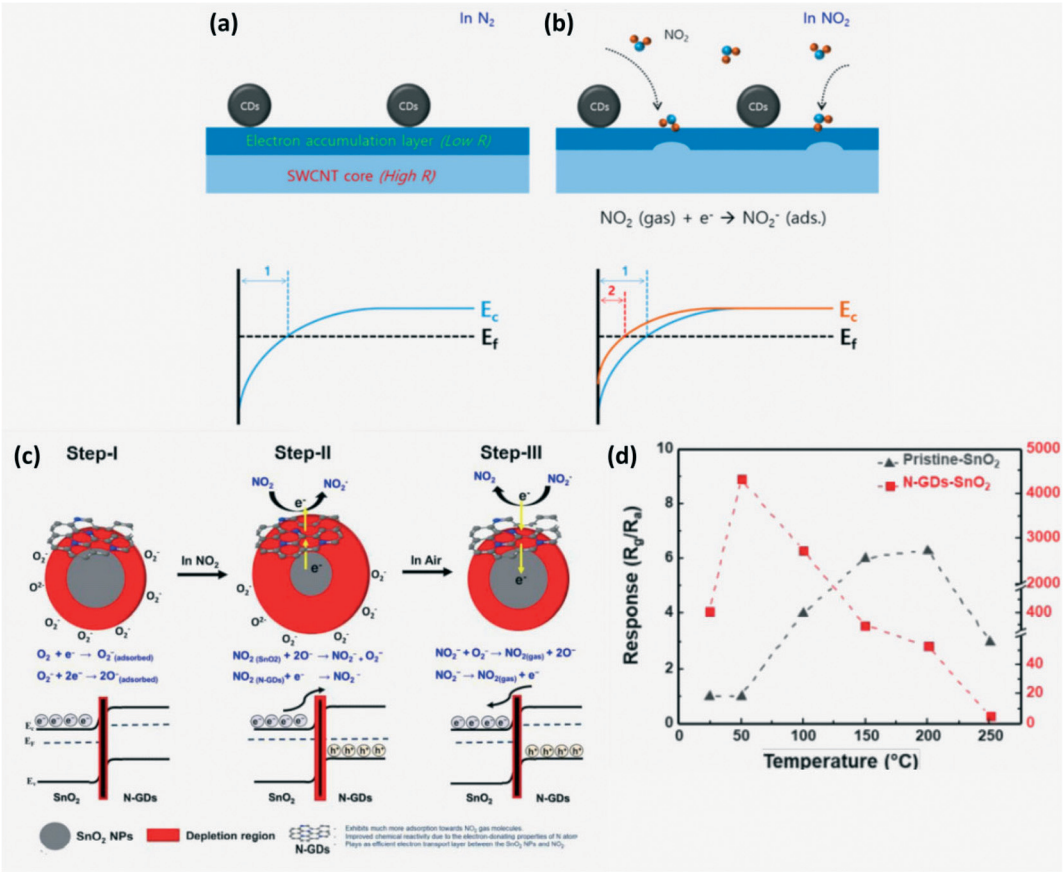

Fig. 22 (a) Schematic of the NO_2 sensing mechanism and electron distribution of SWCNT-CDs in inert atm and (b) in NO_2.[97] Reproduced with permission from ref. 97, copyright, 2020, MDPI. (c) Sensing mechanism of N-GQD/SnO_2 to NO_2; (d) effect of temperature on response of N-GQD/SnO_2 as compared to that of the pristine SnO_2 sensor.[65] Reproduced with permission from ref. 65, copyright, 2020, Royal Society of Chemistry.

higher the number of H^+ ions, the higher the amount of NH_4^+ ions formed which linearly lowers the resistance of the sensor. Hence, sensor response was better at higher relative humidity (Fig. 23A).[67] Chu *et al.*[108] developed a GQDs/ZnO based sensor to detect minute levels of acetic acid at room temperature. A Schottky barrier forms at the ZnO and GQD interface whose height increases on adsorption of oxygen but decreases on adsorption of acetic acid due to the release of the captured electrons to the conduction band as shown by the reaction in eqn (14) and (15). Hence, the resistance of the sensor decreases on exposure to acetic acid.

Similarly, Rahimi & Yazdani[109] developed a ZnO nanorod thin film coated with GQDs as a reducing gas-ethanol sensitive sensor with a similar mechanism of ethanol detection to ZnO/GQD where adsorbed ethanol on the sensor surface reacts with adsorbed O_2 species on ZnO as in eqn (16) resulting in reduced resistance.

$$CH_3COOH_{(ad)} + 2O^{2-}_{(ad)} = 2CO_{2(g)} + 2H_2O_{(g)} + 2e^- \quad (14)$$

$$C_2H_5OH + O^- = CH_3CHO + H_2O + e^- \quad (15)$$

$$CH_3CHO + 5O^- = 2CO_2 + 2H_2O + 5e^- \quad (16)$$

A novel solid-state sensor consisting of N-CDs dispersed over ZnO nanorods grown on a porous Si substrate (NCD-ZnO-pSi) was developed to detect CO_2. NCD-ZnO-pSi has lower surface resistance as compared to pristine ZnO due to higher electron density because of addition of electron rich NCDs which increases sensor response. Addition of NCDs increased O_V density which gave rise to new energy bands and also reduced the crystalline quantity in ZnO structure that serves as the non-radiative defect and as the active site for adsorption. On exposure to CO_2, the resistance of the sensor film increases by formation of (CO_3^{2-}) species which capture electrons from ZnO and increase the Schottky barrier width (Fig. 23C).[70] 20 wt% of graphene/Y_2O_3 QDs developed for CO_2 detection exhibit good stability and the conductivity of the sensor decreases with increasing CO_2 concentration since CO_2 has a tendency to withdraw electrons from the surface through direct adsorption of CO_2 molecules or their reaction with adsorbed oxygen species.[110]

GQDs–SnO_2 co-modified ZnO nanosheets forming an n–p–n heterojunction as shown in Fig. 10 were developed to detect the ppb level of H_2S (reducing gas)[87] and El-Shamy[98] developed a solid state sensor working at room temperature based on CQDs/MgO homogenous film deposited on a p-Si substrate. These sensors followed the mechanism of O_2

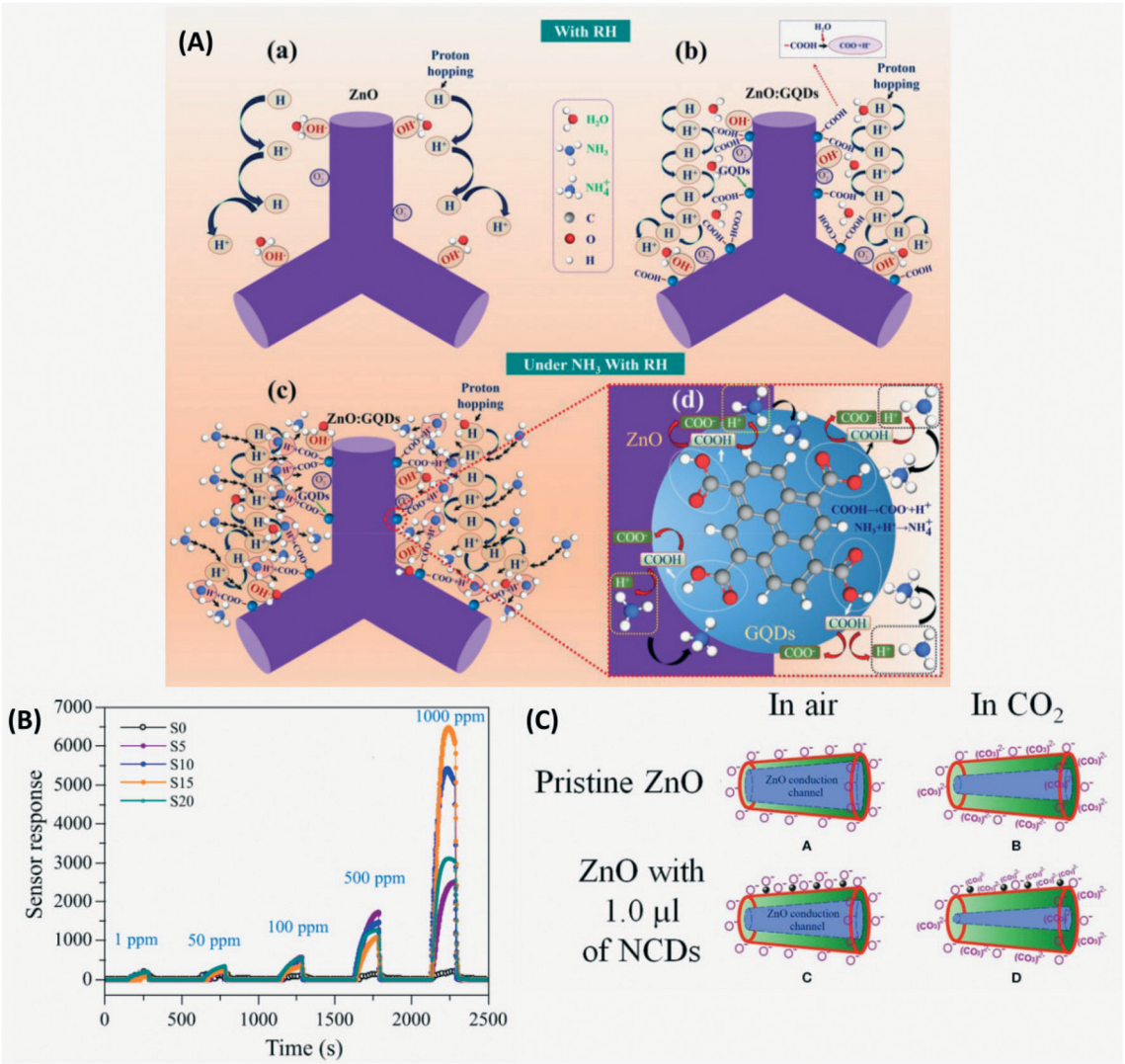

Fig. 23 (A) Schematic of the mechanism of (a) ZnO and (b) ZnO:GQDs under relative humidity, (c) ZnO:GQDs and (d) magnified view of ZnO:GQDs on exposure to NH_3 under relative humidity; (B) response curve of the ZnO–GQDs sensor towards different concentrations of NH_3.[67] Reproduced with permission from ref. 67, copyright, 2021, Elsevier. (C) Schematic diagram of O_2 and CO_2 adsorption on sensors of (A) and (B) ZnO and (C) and (D) ZnO-NCDs respectively.[70] Reproduced with permission from ref. 70, copyright, 2020, Frontiers.

adsorption (traps e^-) leading to reduced electrons in the conduction band which increases the sensor film resistance through widening of the junction potential barrier and desorption of O_2 on exposure to reducing gas such as H_2S, H_2O and SO_2 which releases the trapped e^- and adsorbed oxygen species, reducing the barrier height and eventually resulting in reduced resistance.[87,98] In addition, hole trapping occurs at the MgO–pSi interface which prevents e^-/hole recombination on exposure to H_2S gas and thus increases current. CQDs assist in charge separation and enable electron transfer from MgO to CQDs as there is strong electronic coupling between the conduction bands of MgO and π-electrons in CQDs which enables up-conversion as shown in Fig. 24a.[98]

OH-GQDs which behave as n-type semiconductors have been developed to detect NH_3 gas with high sensitivity and selectivity where upon exposure to NH_3, the sensor resistance decreases rapidly. The sensor resistance recovers to the initial value upon the desorption of NH_3. The NH_3 detection mechanism was attributed to physisorption due to polar interaction and subsequent charge transfer between NH_3 that serves as a donor and the hydroxyl group on the surface of GQDs. Moreover, preference in the adsorption site amongst edge, middle and at the carbon atom along with preferred orientation of NH_3 molecules on approaching the surface of OH-GQDs was evaluated by running a simulation. As observed from Fig. 24b, the nitrogen atom of NH_3 molecules highly prefers to approach the OH molecules at the edge and this is attributed to its increased sensitivity.[21] The SnO_2–GQDs hybrid sensor fabricated by Chu *et al.*[103] and the $ZnFe_2O_4$–GQDs[102] based n-type sensor exhibit increased resistance on adsorption of oxygen due to depletion of electrons in the conduction band, while adsorption of acetone results in dissociation of adsorbed oxygen, thus

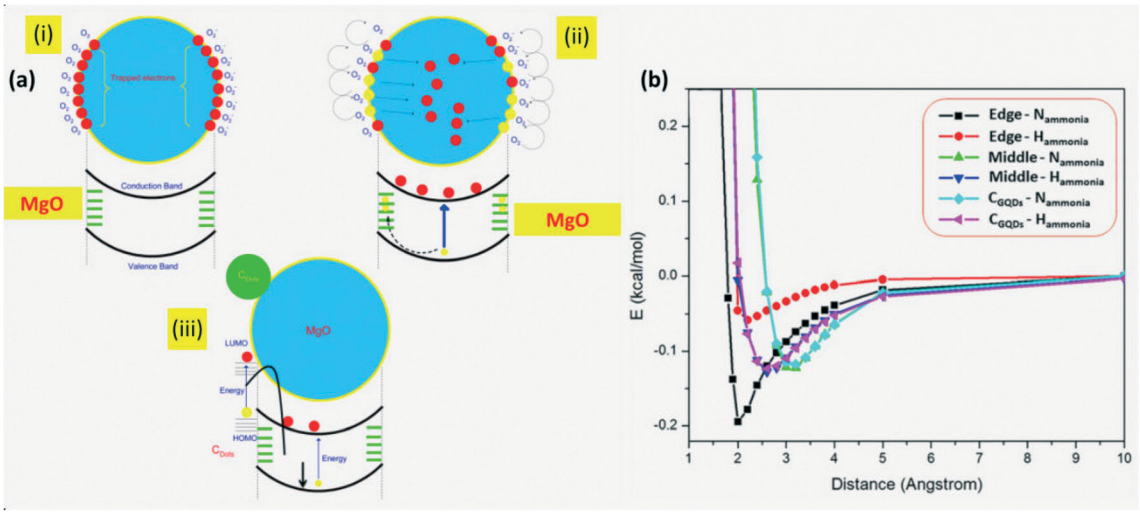

Fig. 24 (a) Schematic diagram of the mechanism of H_2S detection by MgO and MgO-CDs.[98] Reproduced with permission from ref. 98, copyright, 2021, Elsevier. (b) GQDs–NH_3 interaction energies as a function of the adsorption distance for different adsorption sites and configurations.[21] Reproduced with permission from ref. 21, copyright, 2020, Elsevier. (i) Oxygen molecules adsorbed on the MgO surface results in a depletion region, (ii) holes migrate to the surface of MgO and release oxygen ions on adsorption of H_2S gas, (iii) mechanism of carrier transport in CDs@MgO sensor.

returning the captured electrons to the oxide and a decrease in resistance of the sensor film accordingly. The α-Fe_2O_3/GQDs composite sensor developed to detect a highly reducing gas trimethylamine (TMA) works on the same surface charge layer model where adsorption and desorption of O_2 molecules changes the thickness of the potential barrier, the surface charge depletion layer and hence the sensor resistance.[51] The forward biased Schottky barrier formed at the GQDs and MO nanoparticle interface favors faster charge transportation, quick capture and migration of electrons leading to reduced response and recovery time.[51,108]

Embedding NGQDs on TiO_2 nanoplates results in enhanced O_v concentration and favors increased adsorption of O_2. 70% pyridinic N and 30% of graphitic N were found to be present on GQDs which results in p-type NGQDs. Formation of a p–n heterojunction at the NGQDs–TiO_2 interface leads to enhanced photoresponse (7 fold higher compared to TiO_2) through suppression of radiative recombination of charge carriers by effective electron–hole separation through a strong internal electric field. Thus, an improved NO sensing response was observed in NGQDs–TiO_2 sensors in the dark which improved further under UV illumination to 31.1% for 100 ppm NO.[99] Shao *et al.*[111] developed a NGQDs–TiO_2 grafted graphene foam (GF) with improved sensitivity and selectivity for FA. Here initially the sensor surface resistance increases due to depletion of electrons from the TiO_2 surface by adsorbed oxygen. But on exposure to FA, electrons return to the conduction band and resistance decreases (Fig. 25a). A GQDs–TiO_2 nanoporous film was developed for selective detection of isopropanol. The sensor response mechanism and variation in Schottky barrier height on adsorption of oxygen or isopropanol which increases and decreases the film resistance respectively are explained in Fig. 25b.[112]

5. Applications

CD-based sensors are profoundly used to detect volatile organic compounds (VOCs), greenhouse gases and several others as summarized in Table 1 in real time up to very low concentrations as more emphasis is placed on environment monitoring, industrial process control and human health safety. CD-based sensors can be used in one-time alarm application if they possess very long recovery time and as dosimeter-type detectors.[73]

5.1 Detection of VOCs

VOCs beckon grave concerns as they indirectly contribute to global warming, occupational hazards, indoor pollutants, *etc.*[5,19,60,90] One such VOC is NH_3 gas which is widely released from the agricultural sector, livestock, factories leakages, vehicles, *etc.* and is highly toxic at concentrations above 25 ppm on 8 h exposure as it irritates the skin, nose, and eyes, inhibits cell growth, interrupts breathing and causes cancer. But since NH_3 is colorless, it cannot be detected and hence, several methods have been utilized to monitor ammonia levels in air.[19,67,68,73,80,82,100,105] Among these, CD-based resistive gas sensors with low power consumption and cost[67,68,100,105] or optical gas sensors are used for precise measurements of the NH_3 level.[69,72,73,80,82] Acetone is another VOC widely used in pharmaceutical, cosmetics and research industries which is highly volatile and hazardous to human health causing vomiting, headache and may lead to death on exposure to high concentrations.[22,76,84,102,103] They are one of the indoor pollutants along with formaldehyde (FA) and benzene which can be detected at ultra-low concentration using CD-based solid phase sensors.[22] FA, an indoor pollutant commonly released by several home decorations, poses a threat to human health as it can cause blood,

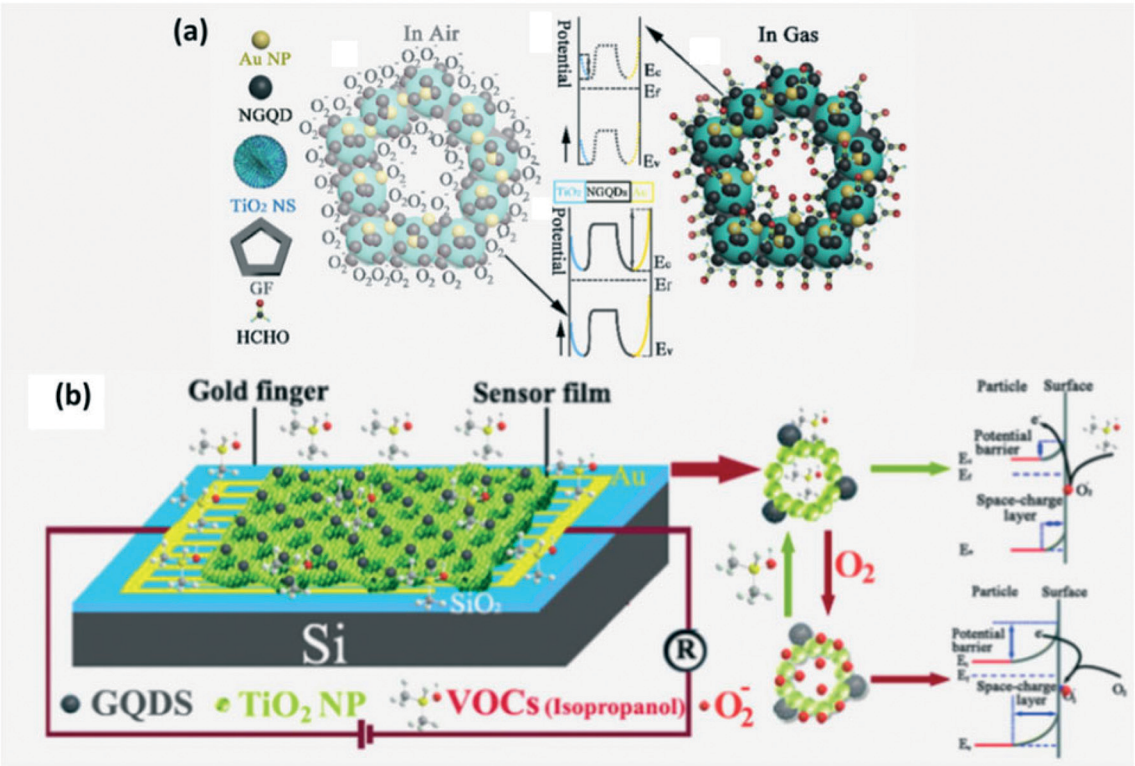

Fig. 25 (a) Schematic diagram of the HCHO sensing mechanism by GF-NGQDs–TiO_2.[111] Reproduced with permission from ref. 111, copyright, 2020, Elsevier. (b) Schematic diagram of the isopropanol sensing mechanism by GQDs–TiO_2.[112] Reproduced with permission from ref. 112, copyright, 2017, Elsevier.

immune and respiratory disorders.[74,111] Thus, their on-site real time detection is of prime importance. Liu *et al.*[74] developed FA responsive building materials from LTW by encapsulating CDs sensitive to FA. A B-GQDs gas sensor was designed for detection of benzene concentration in air which is released through combustion of fuels or from paint. Short term exposure to high benzene concentration may result in drowsiness, skin and eye irritation while long term exposure may lead to lymphoma, leukemia and aplastic anemia.[20] Acetic acid is produced during spoilage of food or combustion of fuels. It is also primarily used in pharmaceuticals, dye and plastic production, *etc.* and real

Table 1 Types of CD-based gas sensors developed recently and their parameters

Material composition	Gas detected	Response time	Recovery time	Limit of detection	Linear range [ppm]	Ref.
GQDs-pH 5	NH_3	26 s	21 s	—	10–400	19
GQDs-pH 7		27 s	72 s	—	10–400	19
OH-GQDs		64 s	69 s	10 ppm	10–500	21
N-GQDs/PANI/		7.0 min	0.083 min	10 ppm	10–1500	105
N-GQDs/PEDOT-PSS		7.7 min	10 min	30 ppm	30–1500	100
CQDs/fluorescein		8 ± 2 min	15 ± 2 min	110 ppb	0.11–200	82
S, N-GQDs/PANI		115 s	44 s	500 ppb	1–1000	68
B-GQDs–$AgLaFeO_3$	HCHO	20–35 s	30–130 s	1 ppm	1–30	27
CQDs	Formic acid	—	52 ± 6 s	7.3% v/v	Up to 100	39
$ZnFe_2O_4$–GQDs	Acetone vapor	<12 s	<12 s	5 ppm	5–1000	102
SnO_2/GQDs		30s	35s	0.1 ppm	0.1–1000	103
GQDs		32 s	48 s	2.5 ppm	2.5–240	22
GQD/MQDs	NO_2	5 min	5 min	41.4 ppb	10–500	106
	NH_3			35.5 ppb	10–500	
GQDs–SnO_2/ZnO	H_2S	14 s	13 s	25 ppb	0.025–5	87
In_2O_3/CD hybrids	NO_2	9.6 min	5.3 min	50 ppb	0.05–0.5	104
N-GQD/SnO_2		181 s	81 s	20 ppb	0.02–0.2	65
CDs/SWCNTs		381 s	294 s	18 ppb	0.1–4.5	97
ZnO/GQDs	Acetic acid	43 s	49 s	1 ppm	1–1000	108
Fe_2O_3/GQDs	TMA	11 s	24 s	0.01 ppm	0.01–1000	51
CD	NO_2	150 s	315 s	50 ppb	0.14–2.5	107

time detection of acetic acid vapor has been easily realized using a CD sensor since continuous exposure to acetic acid vapors is considered hazardous to human health and may cause teeth erosion.[45,71,108]

CDs can also be used in an optical electronic nose system which mimics the function of the olfactory system in humans (Fig. 26). In an optoelectronic nose, changes in absorbance or emission intensity of the sensor material are converted into electrical signals which can be analyzed using principal component analysis (PCA) to identify the target gas. These devices can be used for environmental monitoring, pharmaceuticals, food or beverage testing and clinical applications.[39,45,69,76,78] Although formic acid as the simplest volatile carboxylic acid is used as a precursor to synthesize several products such as antibacterial agents and preservatives, on exposure to increased doses, it leads to irritation, blindness and nerve damage and hence a CD-based optical electronic nose system was developed to keep the vapor level in the surroundings in check.[39]

Excessive accumulation of methanol or ethanol in the human body may cause irritation or intoxication or even lead to death. Thus, an optoelectronic nose based on CDs prepared by green synthesis was used to detect alcohol vapor by observing variation in absorbance of CDs on exposure to vapors.[78] Nitrites are one of the essential components for the formation of carcinogenic *N*-nitrosamine and thus it is necessary to detect alarming amounts of nitrites if present in water, milk or any other food.[23] Phenol and phenolic molecules such as 2,4-dinitrophenol (DNP) widely used in pharmaceuticals, dyes and pesticides are common industrial effluents hazardous to human and animal health even at low concentration. Hence a CQDs-MOF composite was developed to monitor their concentration in air.[93] Another important aromatic compound, aniline is highly toxic even in trace amounts and exposure to its vapors can cause chronic poisoning. Ma *et al.*[83] developed a CQD/silica aerogel composite sensor to detect the presence of aniline.

5.2 Detection of toxic gas pollutants

It is necessary to detect greenhouse gases and toxic gases that result in environmental degradation, acid rain and ozone depletion. A greenhouse gas, CO_2 emitted into air through combustion, respiration, *etc.*, can be sensed using CDs. CO_2 may act as an oxidizing or reducing gas depending on the chemical structure of sensor materials.[18,30,88,110] NO/NO_2 is considered to be a source of photochemical smog, acid rain and particulate matter detrimental to the human respiratory system which at very high concentration may lead to death due to asphyxia and can be detected using CDs.[65,66,86,97,99,104,107,113] H_2S gas is highly inflammable, irritant, toxic and corrosive.[98] Even trace concentration can cause distress while exposure to high concentration may cause unconsciousness, brain damage or cell death by asphyxia.[94] Industries such as paper mills, oil or gas producers are the main source of H_2S along with sewage treatment plants. A solid state H_2S sensor of CQDs/MgO homogenous film deposited on a p-Si substrate[98] and a N-CQDs/Ag nanoparticle[94] based sensor were developed in order to monitor the level of H_2S in the environment. CD-based sensors have been developed for analyzing food quality by functional component analysis such as quercetin or curcumin[16,32] and detection of harmful or hazardous additives or pesticides.[13,14,16,28] Recently, α-Fe_2O_3/GQDs based gas sensors were fabricated to help recognize the freshness of fish to protect human health and the environment through sensing of trimethylamine (TMA) gas which is released by dead fish.[51,96]

5.3 Diagnosis of diseases

CDs can be adopted as sensor materials instead of semiconductor quantum dots in flexible gas sensors[113] and breathalyzers as they have low toxicity and are biocompatible. Carbon dots in conjunction with polymers or semiconductor MOs have been used to synthesize a breathalyzer, a gas sensor for analyzing the breath of human beings containing various chemicals in a non-invasive manner, to predict an underlying disease, disorders or deficiency in the human body.[60,67,69,87,103] For instance, humans with obesity or diabetes tend to have high acetone levels in their blood and breath (>1.8 ppm) and thus qualitative and quantitative detection of acetone can be used for diagnosing such underlying diseases.[22,76,103] The presence of ammonia in

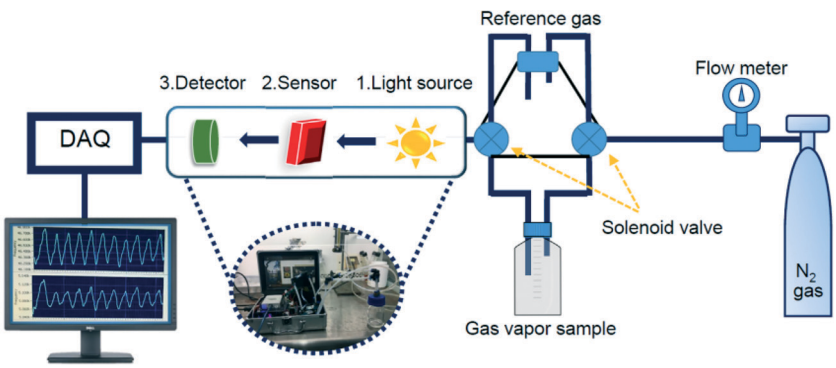

Fig. 26 Schematic explaining the function of the optoelectronic nose.[39] Reproduced with permission from ref. 39, copyright, 2018, Elsevier.

breath is an indication of stomach ulcer while the presence of NO may serve as an indication of asthma.[60,99] The presence of more than 0.1 ppm H_2S in exhalation of a human is indicative of halitosis,[87] while the presence of TMA in human breath is an indication of renal disease.[51] The presence of FA in human breath is an indicator of lung cancer since the amount of FA in exhaled breath of healthy patients generally is less than 48 ppb. For this reason, a GF-NGQDs–TiO_2 based sensor was developed with the ability to sense 40 ppb FA with a good response.[111] CDs can be synthesized using a facile green method and they are eco-friendly and thus CD-based gas sensors can be adopted to detect VOCs, air pollutants and in breathalyzers. However, highly sensitive, selective and stable CDs required to probe and detect specific gas molecules demand more stringent synthesis conditions. Further optimization of the sensing conditions is also required.

6. Conclusions

MO nanoparticle, conducting polymer, aerogel and other carbon nanomaterial-based sensor films suffer from poor sensitivity to target molecules. To overcome their limitations, CDs have been adopted as an effective active material. CDs possess lucrative optical and electrical properties which can be fine-tuned with precision by surface passivation, doping and controlling the degree of carbonization during synthesis. Thus, a wide variety of solid phase and solution phase gas sensors have been developed by researchers by exploiting their advantageous luminescence and conductivity. Initially simple, pristine and surface passivated CD-based optical gas sensors were developed which was followed by deliberately doped CD-based optical and resistive gas sensors to achieve higher sensitivity and selectivity to target gas molecules. At present, CDs in conjunction with aforementioned sensor film-based gas sensors with improved response and recovery at room temperature have been successfully developed. Currently, multi-gas sensing films and multi array gas sensors based on CDs are also being explored. Gas sensors are eminent in our current society as they can help to curb major disasters by alerting people regarding the possible outbreak of toxic, inflammable or hazardous gases in industries and also help to detect environmentally toxic gases such as greenhouse gases, indoor pollutants, *etc.* Furthermore, some of the gas molecules in our breath serve as indicators of underlying diseases. So, analyzing human breath can help in early diagnosis in order to provide effective medication and treatment. Despite these advantages of CD-based gas sensors, some of the limitations are: CDs synthesized from natural precursors possess low QY and chemical inhomogeneity; pH and temperature dependent response of CDs needs to be addressed along with the need to obtain better insight into their sensing mechanism. Further efforts are being expended to develop a stable, reversible and highly selective and sensitive gas sensor operating at room temperature. Hence, we believe CDs possess a lot of potential as an active material in gas sensors as they have all the necessary properties such as a large surface area, conductivity and selective reactive sites that can be obtained *via* surface passivation for effective and efficient gas sensing.

Conflicts of interest

There are no conflicts to declare.

References

1 S. Gogoi, M. Kumar, B. B. Mandal and N. Karak, *RSC Adv.*, 2016, **6**, 26066–26076.
2 J. Shen, Y. Zhu, X. Yang and C. Li, *Chem. Commun.*, 2012, **48**, 3686–3699.
3 X. Xu, R. Ray, Y. Gu, H. J. Ploehn, L. Gearheart, K. Raker and W. A. Scrivens, *J. Am. Chem. Soc.*, 2004, **126**, 12736–12737.
4 S. Sagbas and N. Sahiner, Carbon Dots: Preparation, Properties, and Application, *Nanocarbon and Its Composites*, Elsevier, 2019, pp. 651–676.
5 M. Zheng, Y. Li, Y. Zhang and Z. Xie, *RSC Adv.*, 2016, **6**, 83501–83504.
6 M. L. Liu, B. B. Chen, C. M. Li and C. Z. Huang, *Green Chem.*, 2019, **21**, 449–471.
7 M. Moorthy, V. B. Kumar, Z. Porat and A. Gedanken, *New J. Chem.*, 2018, **42**, 535–540.
8 L. Li, J. Li, R. Fei, C. Wang, Q. Lu, J. Zhang, L. Jiang and J. Zhu, *Adv. Funct. Mater.*, 2012, **22**, 2971–2979.
9 B. Yao, H. Huang, Y. Liu and Z. Kang, *Trends Chem.*, 2019, **1**, 235–246.
10 X. Ma, S. Li, V. Hessel, L. Lin, S. Meskers and F. Gallucci, *Chem. Eng. Process.*, 2019, **140**, 29–35.
11 A. Dager, T. Uchida, T. Maekawa and M. Tachibana, *Sci. Rep.*, 2019, **9**, 14004.
12 C. Xia, S. Zhu, T. Feng, M. Yang and B. Yang, *Adv. Sci.*, 2019, **6**, 1901316.
13 Y. R. Kumar, K. Deshmukh, K. K. Sadasivuni and S. K. K. Pasha, *RSC Adv.*, 2020, **10**, 23861–23898.
14 N. Dhenadhayalan, K. Lin and T. A. Saleh, *Small*, 2019, **16**, 1905767.
15 X. Wang, Y. Feng, P. Dong and J. Huang, *Front. Chem.*, 2019, **7**, 671.
16 M. Pan, X. Xie, K. Liu, J. Yang, L. Hong and S. Wang, *Nanomaterials*, 2020, **10**, 930.
17 F. Yuan, T. Yuan, L. Sui, Z. Wang, Z. Xi, Y. Li, X. Li, L. Fan, Z. Tan, A. Chen, M. Jin and S. Yang, *Nat. Commun.*, 2018, **9**, 2249.
18 D. Raeyani, S. Shojaei, S. A. Kandjani and W. Wlodarski, *Procedia Eng.*, 2016, **168**, 1312–1316.
19 W. Chen, F. Li, P. C. Ooi, Y. Ye, T. W. Kim and T. Guo, *Sens. Actuators, B*, 2016, **222**, 763–768.
20 Y. Zhang, Q. Rong, J. Zhao, J. Zhang, Z. Zhu and Q. Liu, *J. Mater. Chem. A*, 2018, **6**, 12647–12653.
21 S. Arunragsa, Y. Seekaw, W. Pon-On and C. Wongchoosuk, *Diamond Relat. Mater.*, 2020, **105**, 107790.

22 J. Wang, S. Lin, Y. Lin and X. Wang, *Sens. Mater.*, 2021, **33**, 499–511.
23 Z. Lin, W. Xue, H. Chen and J. Lin, *Anal. Chem.*, 2011, **83**, 8245–8251.
24 J. Zhang and S. Yu, *Mater. Today*, 2016, **19**, 382–393.
25 C. Li, C. Ou, C. Huang, W. Wu, Y. Chen, T. Lin, L. Ho, C. Wang, C. Shih, H. Zhou, Y. Lee, W. Tzeng, T. Chiou, S. Chu, J. Cang and H. T. Chang, *J. Mater. Chem. B*, 2014, **2**, 4564–4571.
26 A. A. Ensafi, S. H. Sefat, N. Kazemifard, B. Rezaei and F. Moradi, *Sens. Actuators, B*, 2017, **253**, 451–460.
27 Y. Zhang, J. Zhao, H. Sun, Z. Zhu, J. Zhang and Q. Liu, *Sens. Actuators, B*, 2018, **266**, 364–374.
28 T. Ghiasi, S. Ahmadi, E. Ahmadi, M. Olyai and Z. Khodadadi, *Microchem. J.*, 2021, **160**, 105628.
29 M. Li, T. Chen, J. J. Gooding and J. Liu, *ACS Sens.*, 2019, **4**, 1732–1748.
30 D. Raeyani, S. Shojaei and S. A. Kandjani, *Mater. Res. Express*, 2020, **7**(1), 015608.
31 X. Zhang, Y. Zhang, Y. Wang, S. Kalytchuk, S. V. Kershaw, Y. Wang, P. Wang, T. Zhang, Y. Zhao, H. Zhang, T. Cui, Y. Wang, J. Zhao, W. W. Yu and A. L. Rogach, *ACS Nano*, 2013, **7**, 11234–11241.
32 P. Zhao, M. Ni, Y. Xu, C. Wang, C. Chen, X. Zhang, C. Li, Y. Xie and J. Fei, *Sens. Actuators, B*, 2019, **299**, 126997.
33 X. Huang, L. Jin, C. Wang, Y. Xu, P. Zhou, M. Xie, C. Zhang, W. Yang and J. Lu, *Compos. Commun.*, 2020, **20**, 100348.
34 S. Bhattacharya, R. S. Phatake, S. N. Barnea, N. Zerby, J. Zhu, R. Shikler, N. G. Lemcoff and R. Jelinek, *ACS Nano*, 2019, **13**, 1433–1442.
35 C. Zhu, Y. Fu, C. Liu, Y. Liu, L. Hu, J. Liu, I. Bello, H. Li, N. Liu, S. Guo, H. Huang, Y. Lifshitz, S. Lee and Z. Kang, *Adv. Mater.*, 2017, **29**, 1701399.
36 S. Zhu, Q. Meng, L. Wang, J. Zhang, Y. Song, H. Jin, K. Zhang, H. Sun, H. Wang and B. Yang, *Angew. Chem., Int. Ed.*, 2013, **52**, 3953–3957.
37 X. Cui, Y. Wang, J. Liu, Q. Yang, B. Zhang, Y. Gao, Y. Wang and G. Lu, *Sens. Actuators, B*, 2017, **242**, 1272–1280.
38 F. Zu, F. Yan, Z. Bai, J. Xu, Y. Wang, Y. Huang and X. Zhou, *Microchim. Acta*, 2017, **184**, 1899–1914.
39 S. Moonrinta, B. Kwon, I. In, S. Kladsomboon, W. Sajomsang and P. Paoprasert, *Opt. Mater.*, 2018, **81**, 93–101.
40 S. Yang, J. Sun, X. Li, W. Zhou, Z. Wang, P. He, G. Ding, X. Xie, Z. Kang and M. Jiang, *J. Mater. Chem. A*, 2014, **2**, 8660–8667.
41 H. Liu, J. Ding, K. Zhang and L. Ding, *TrAC, Trends Anal. Chem.*, 2019, **118**, 315e337.
42 Q. Huanga, Q. Lia, Y. Chena, L. Tongc, X. Lina, J. Zhua and Q. Tong, *Sens. Actuators, B*, 2018, **276**, 82–88.
43 H. M. Junaid, A. R. Solangib and M. Batool, *Analyst*, 2021, **146**, 2463–2474.
44 H. Abdolmohammad-Zadeh, Z. Azari and E. Pourbasheer, *Spectrochim. Acta, Part A*, 2021, **245**, 118924.
45 J. Praneerad, N. Thongsai, P. Supchocksoonthorn, S. Kladsomboon and P. Paoprasert, *Spectrochim. Acta, Part A*, 2019, **211**, 59–70.
46 G. Huang, X. Luo, W. Lin, W. Tang, T. Yue, J. Wang and Z. Li, *Dyes Pigm.*, 2022, **203**, 110381.
47 A. Abbasi and M. Shakir, *Sens. Diagn.*, 2022, **1**, 516.
48 V. Ruiz, I. Fernandez, P. Carrasco, G. Cabanero, H. J. Grande and J. Herran, *Sens. Actuators, B*, 2015, **218**, 73–77.
49 P. Chaudhary, D. K. Maurya, S. Yadav, A. Pandey, R. K. Tripathi and B. C. Yadav, *Sens. Actuators, B*, 2021, **329**, 129116.
50 K. Jlassi, S. Mallick, A. Eribi, M. M. Chehimi, Z. Ahmad, F. Touati and I. Krupa, *Sens. Actuators, B*, 2021, **328**, 129058.
51 T. Hu, X. Chu, F. Gao, Y. Dong, W. Sun and L. Bai, *J. Solid State Chem.*, 2016, **237**, 284–291.
52 B. Wu, G. Zhu, A. Dufresne and N. Lin, *ACS Appl. Mater. Interfaces*, 2019, **11**, 16048–16058.
53 A. Abbasi and M. Shakir, *J. Fluoresc.*, 2022, **32**, 1239–1246.
54 X. Lin, M. Xiong, J. Zhang, C. He, X. Ma, H. Zhang, Y. Kuang, M. Yang and Q. Huang, *Microchem. J.*, 2021, **160**, 105604.
55 Q. Huang, X. Lin, L. Tong and Q.-X. Tong, *ACS Sustainable Chem. Eng.*, 2020, **8**, 1644–1650.
56 S. Bilal, A. J. Sami, A. Hayat and M. F. Rehman, *Bioelectrochemistry*, 2022, **144**, 107999.
57 Q. Huanga, X. Lina, J.-J. Zhua and Q.-X. Tong, *Biosens. Bioelectron.*, 2017, **94**, 507–512.
58 Q. Huang, X. Lin, D. Chen and Q.-X. Tong, *Food Chem.*, 2022, **373**, 131415.
59 X. Li, X. Xing, S. Zhao, S. Zhu, B. Wang, M. Lan and X. Song, *Chin. Chem. Lett.*, 2022, **33**, 1632–1636.
60 J. Hodgkinson, J. Saffell, J. Luff, J. Shaw, J. Ramsden, C. Huggins, R. Bogue and R. Carline, *Nanotechnol. Perceptions*, 2009, **5**(1), 71–82.
61 Z. Yunusa, M. H. Hamidon, A. Kaiser and Z. Awang, *Sens. Transducers*, 2014, **168**, 61–75.
62 M. Penza, P. J. Martin and J. T. W. Yeow, Carbon Nanotube Gas Sensors. *Gas Sensing Fundamentals, Springer Series on Chemical Sensors and Biosensors*, ed. C. D. Kohl and T. Wagner, Springer, Berlin, Heidelberg, 2014, vol. 15.
63 A. O. Idris, E. O. Oseghe, T. A. M. Msagati, A. T. Kuvarega, U. Feleni and B. Mamba, *Sensors*, 2020, **20**, 5743.
64 D. J. Buckley, N. C. G. Black, E. G. Castanon, C. Melios, M. Hardman and O. Kazakova, *2D Mater.*, 2020, **7**, 032002.
65 R. Purbia, Y. M. Kwon, H. D. Kim, Y. S. Lee, H. Shin and J. M. Baik, *J. Mater. Chem. A*, 2020, **8**, 11734–11742.
66 W. Jiang, X. Chen, T. Wang, B. Li, M. Zeng, J. Yang, N. Hu, Y. Su, Z. Zhou and Z. Yang, *RSC Adv.*, 2021, **11**, 5618–5628.
67 E. Wongrat, T. Nuengnit, R. Panyathip, N. Chanlek, N. Hongsith and S. Choopun, *Sens. Actuators, B*, 2021, **326**, 128983.
68 J. N. Gavgani, A. Hasani, M. Nouri, M. Mahyari and A. Salehi, *Sens. Actuators, B*, 2016, **229**, 239–248.
69 P. Supchocksoonthorn, N. Thongsai, H. Moonmuang, S. Kladsomboon, P. Jaiyong and P. Paoprasert, *Colloids Surf., A*, 2019, **575**, 118–128.
70 J. A. Ramos-Ramón, N. K. R. Bogireddy, J. A. G. Vieyra, T. V. K. Karthik and A. Agarwal, *Front. Chem.*, 2020, **8**, 291.
71 M. Wang, Y. Xia, J. Qui and X. Ren, *Spectrochim. Acta, Part A*, 2019, **206**, 170–176.
72 B. Jiang, B. Zhou, X. Shen, Y. Yu, S. Ji, C. Wen and H. Liang, *Chem. – Eur. J.*, 2015, **21**, 18993–18999.

73 N. A. Travlou, J. Secor and T. J. Bandosz, *Carbon*, 2017, **114**, 544–556.
74 Y. Liu, H. Yang, C. Ma, S. Luo, M. Xu, Z. Wu, W. Li and S. Liu, *ACS Appl. Mater. Interfaces*, 2020, **12**, 36628–36638.
75 B. Lei, L. Wang, H. Zhang, Y. Liu, H. Dong, M. Zheng and X. Zhou, *Sens. Actuators, B*, 2016, **230**, 101–108.
76 N. Thongsai, P. Jaiyong, S. Kladsomboon, I. In and P. Paoprasert, *Appl. Surf. Sci.*, 2019, **487**, 1233–1244.
77 Y. He, J. He, L. Wang, Z. Yu, H. Zhang, Y. Liu and B. Lei, *Sens. Actuators, B*, 2017, **251**, 918–926.
78 N. Thongsai, N. Tanawannapong, J. Praneerad, S. Kladsomboon, P. Jaiyong and P. Paoprasert, *Colloids Surf., A*, 2019, **560**, 278–287.
79 J. Hu, C. Zou, Y. Su, M. Li, N. Hu, N. Hui, Z. Yang and Y. Zhang, *J. Mater. Chem. C*, 2017, **5**, 6862–6871.
80 M. Ganiga and J. Cyriac, *Sens. Actuators, B*, 2016, **225**, 522–528.
81 B. Chen, S. Chai, J. Liu, C. Liu, Y. Li, J. He, Z. Yu, T. Yang, C. Feng and C. Huang, *Anal. Bioanal. Chem.*, 2019, **411**, 2291–2300.
82 C.-P. Hsu, Z. Hejazi, E. Armagan, S. Zhao, M. Schmid, H. Zhang, H. Guo, L. Weidenbacher, R. M. Rossi, M. M. Koebel, L. F. Boesel and C. Toncelli, *Sens. Actuators, B*, 2017, **253**, 714–722.
83 Y. Ma, X. Chen, J. Bai, G. Yuan and L. Ren, *Inorg. Chem. Commun.*, 2019, **100**, 64–69.
84 Y. Liu, W. Li, P. Wu, C. Ma, X. Wu, M. Xu, S. Luo, Z. Xu and S. Liu, *Sens. Actuators, B*, 2019, **281**, 34–43.
85 S. Zhu, Y. Song, X. Zhao, J. Shao, J. Zhang and B. Yang, *Nano Res.*, 2015, **8**, 355–381.
86 R. Wang, G. Li, Y. Dong, Y. Chi and G. Chen, *Anal. Chem.*, 2013, **85**, 8065–8069.
87 S. Shao, X. Chen, Y. Chen, L. Zhang, H. W. Kim and S. S. Kim, *ACS Appl. Nano Mater.*, 2020, **3**, 5220–5230.
88 D. Raeyani, S. Shojaei and S. Ahmadi-Kandjani, *Superlattices Microstruct.*, 2018, **114**, 321–330.
89 X. Sun and L. Yu, *TrAC, Trends Anal. Chem.*, 2017, **89**, 163–180.
90 S. Dolai, S. K. Bhunia and R. Jelinek, *Sens. Actuators, B*, 2017, **241**, 607–613.
91 X. Yan, Y. Song, C. Zhu, H. Li, D. Du, X. Su and Y. Lin, *Anal. Chem.*, 2018, **90**, 2618–2624.
92 L. Wang, H. Zhang, X. Zhou, Y. Liu and B. Lei, *J. Colloid Interface Sci.*, 2016, **478**, 256–262.
93 J. Yang and Y. Kou, *Inorg. Chim. Acta*, 2021, **519**, 120276.
94 C. Wang, Y. Ding, X. Bi, J. Luo, G. Wang and Y. Lin, *Sens. Actuators, B*, 2018, **264**, 404–409.
95 S. Bhattacharya, R. Sarkar, B. Chakraborty, A. Porgador and R. Jelinek, *ACS Sens.*, 2017, **2**, 1215–1224.
96 L. Liu, S. Fu, X. Lv, L. Yue, L. Fan, H. Yu, X. Gao, W. Zhu, W. Zhang, X. Li and W. Zhu, *Front. Bioeng. Biotechnol.*, 2020, **8**, 567584.
97 N. Lim, J. Lee and Y. T. Byun, *Nanomaterials*, 2020, **10**, 2509.
98 A. G. El-Shamy, *Sens. Actuators, B*, 2021, **329**, 129154.
99 G. Murali, M. Redeppa, C. H. Reddy, S. Park, T. Chandrakalavathit, M. Kim and I. In, *ACS Appl. Mater. Interfaces*, 2020, **12**, 13428–13436.
100 M. Hakimi, A. Salehi and F. A. Boroumand, *IEEE Sens. J.*, 2016, **16**, 6149–6154.
101 F. Montejo-Alvaro, J. Oliva, M. Herrera-Trejo, H. M. Garcia and A. I. Mtz-Enriquez, *Theor. Chem. Acc.*, 2019, **138**, 37.
102 X. Chu, P. Dai, S. Liang, A. Bhattacharya, Y. Dong and M. Epifani, *Phys. E*, 2019, **106**, 326–333.
103 X. Chu, J. Wang, J. Zhang, Y. Dong, W. Sun, W. Zhang and L. Bai, *J. Mater. Sci.*, 2017, **52**, 9441–9451.
104 M. Cheng, Z. Wu, G. Liu, L. Zhao, Y. Gao, S. Li, B. Zhang, X. Yan and G. Lu, *Sens. Actuators, B*, 2020, **304**, 127272.
105 M. Hakimi, A. Salehi, F. A. Boroumand and N. Mosleh, *IEEE Sens. J.*, 2018, **18**, 2245–2252.
106 N. Yue, W. Rongguo, J. Weicheng, D. Guomin and H. Yifan, *J. Mater. Chem. A*, 2016, **4**, 8198–8203.
107 S. Sawalha, K. Moulaee, G. Nocito, A. Silvestri, S. Petralia, M. Prato, S. Bettini, L. Valli, S. Conoci and G. Neri, *Carbon Trends*, 2021, **5**, 100105.
108 X. Chu, P. Dai, Y. Dong, W. Sun, L. Bai and W. Zhang, *J. Mater. Sci.: Mater. Electron.*, 2017, **28**, 19164–19173.
109 K. Rahimi and A. Yazdani, *Mater. Lett.*, 2018, **228**, 65–67.
110 K. R. Nemade and S. A. Waghuley, *Int. J. Mod. Phys.: Conf. Ser.*, 2013, **22**, 380–384.
111 S. Shao, H. W. Kim, S. S. Kim, Y. Chen and M. Lai, *Appl. Surf. Sci.*, 2020, **516**, 145932.
112 S. Shao, W. Wang, K. Zhou, F. Jiang, H. Wu and R. Koehn, *Mater. Lett.*, 2017, **186**, 193–197.
113 Z. Song, Z. Huang, J. Liu, Z. Hu, J. Zhang, G. Zhang, F. Yi, S. Jiang, J. Lian, J. Yan, J. Zang and H. Liu, *ACS Sens.*, 2018, **3**, 1048–1055.